RESEARCH ARTICLE

Woody Encroachment Modifies Subsurface Structure and Hydrological Function

Karla M. Jarecke[1] 🔵 | Xi Zhang[2] | Rachel M. Keen[3] 🔵 | Marc Dumont[4] 🔵 | Bonan Li[1] | Kayalvizhi Sadayappan[5] | Victoria Moreno[1] | Hoori Ajami[6] | Sharon A. Billings[3] | Alejandro N. Flores[7] | Daniel R. Hirmas[8] | Matthew F. Kirk[9] 🔵 | Li Li[5] | Jesse B. Nippert[10] | Kamini Singha[4] | Pamela L. Sullivan[1]

[1]College of Earth, Ocean, and Atmospheric Sciences, Oregon State University, Corvallis, Oregon, USA | [2]Red River Research Station and School of Plant, Environmental, and Soil Sciences, Louisiana State University-Agricultural Center, Baton Rouge, Louisiana, USA | [3]Department of Ecology and Evolutionary Biology and Kansas Biological Survey and Center for Ecological Research, University of Kansas, Lawrence, Kansas, USA | [4]Hydrologic Science and Engineering Program, Colorado School of Mines, Golden, Colorado, USA | [5]Department of Civil and Environmental Engineering, The Pennsylvania State University, University Park, Pennsylvania, USA | [6]Department of Environmental Sciences, University of California Riverside, California, Riverside, USA | [7]Department of Geosciences, Boise State University, Boise, Idaho, USA | [8]Department of Plant and Soil Science, Texas Tech University, Lubbock, Texas, USA | [9]Department of Geology, Kansas State University, Manhattan, Kansas, USA | [10]Division of Biology, Kansas State University, Manhattan, Kansas, USA

Correspondence: Karla M. Jarecke (karla.jarecke@oregonstate.edu)

ABSTRACT

Woody encroachment—the expansion of woody shrubs into grasslands—is a widely documented phenomenon with global significance for the water cycle. However, its effects on watershed hydrology, including streamflow and groundwater recharge, remain poorly understood. A key challenge is the limited understanding of how changes to root abundance, size and distribution across soil depths influence infiltration and preferential flow. We hypothesised that woody shrubs would increase and deepen coarse-root abundance and effective soil porosity, thus promoting deeper soil water infiltration and increasing soil water flow velocities. To test this hypothesis, we conducted a study at the Konza Prairie Biological Station in Kansas, where roughleaf dogwood (*Cornus drummondii*) is the predominant woody shrub encroaching into native tallgrass prairie. We quantified the distribution of coarse and fine roots and leveraged soil moisture time series and electrical resistivity imaging to analyse soil water flow beneath shrubs and grasses. We observed a greater fraction of coarse roots beneath shrubs compared to grasses, which was concurrent with greater saturated hydraulic conductivity and effective porosity. Half-hourly rainfall and soil moisture data show that the average soil water flow through macropores was 135% greater beneath shrubs than grasses at the deepest B horizon, consistent with greater saturated hydraulic conductivity. Soil-moisture time series and electrical resistivity imaging also indicated that large rainfall events and greater antecedent wetness promoted more flow in the deeper layers beneath shrubs than beneath grasses. These findings suggest that woody encroachment alters soil hydrologic processes with cascading consequences for ecohydrological processes, including increased vertical connectivity and potential groundwater recharge.

1 | Introduction

Increasing rates of woody encroachment, where woody plants increase in density and cover in native grasslands or rangelands, have been a global phenomenon in the last century (Deng et al. 2021). Woody encroachment is promoted by fire suppression, overgrazing and changes in precipitation regimes (Archer et al. 2017; D'Odorico, Okin, and Bestelmeyer 2012; García Criado et al. 2020; Jurena and Archer 2003; Twidwell et al. 2013; Van Auken 2009) and has led to unexpected and mixed hydrological changes across diverse ecosystems. For example, concurrent climate change and woody encroachment reduced annual streamflow despite more than 100 years of increased precipitation in mesic grasslands (Keen et al. 2022; Sadayappan et al. 2023). This outcome may be attributed, in part, to increased evapotranspiration (ET) (O'Keefe et al. 2020) and elevated soil drying with increased woody cover (Craine and Nippert 2014). Conversely, in other ecosystems, woody encroachment has increased annual streamflow due to relatively constant ET but increased soil infiltrability and groundwater recharge (Wilcox et al. 2022). Key factors in these observed differences include climate, bedrock composition and vadose zone characteristics. However, the mechanisms by which woody encroachment modifies subsurface hydrologic processes across these factors are not fully understood (Huxman et al. 2005; Keen et al. 2024).

Increasing woody cover across diverse ecotones is altering hydrological connectivity, defined here as the extent to which water can be redistributed through the landscape (Wilcox et al. 2022). One mechanism by which woody encroachment is shifting vertical hydrological connectivity belowground is through the growth of woody-plant roots. Roots help shape subsurface hydraulic properties and their distribution and size can impact the flow and storage of water, carbon, and nutrients (Sullivan et al. 2022). Woody encroachment has potentially led to significant deepening of root systems across 35% of Earth's terrestrial surface (Hauser et al. 2022). Both the occurrence of roots in deeper soil volumes and changes in root sizes can impact soil structure and soil hydraulic properties (Lu et al. 2020; Scholl et al. 2014). Roots can directly control water flow by creating macropores that promote preferential flow, defined as the rapid channelling of water through a relatively small portion of soil-pore space that bypasses a drier soil matrix (Nimmo 2021). Live roots develop saturated films on their surface that increase water flow (Bogner et al. 2010), and decayed roots leave behind tissue that coats channel walls and enhances water flow (Angers and Caron 1998). Preferential flow has been observed along laterally oriented coarse roots (Guo et al. 2020) as well as vertically oriented coarse roots that can shunt water to deeper soil layers (Li et al. 2009; Schwärzel, Ebermann, and Schalling 2012). Moreover, increased root density and root biomass tend to be greater in preferential flow pathways than in the surrounding soil matrix (Bogner et al. 2010; Y. Zhang et al. 2015), suggesting that root systems, including fine roots, play an important role in soil water flow and nutrient and solute transport.

Roots can indirectly influence soil structure through the release of organic material. Root exudates can enmesh soil particles and stabilise aggregates, which can increase soil permeability (Denef et al. 2002; Gyssels et al. 2005). In contrast, root growth can also clog existing pores and break down macroaggregates, which can decrease soil permeability. However, the presence of roots tends to increase porosity and enhance water flow more often than it reduces pore space (Sullivan et al. 2022). Relatively small increases in soil macroporosity can have large effects on saturated hydraulic conductivity (Eck et al. 2016; Lu et al. 2020). Thus, changes in rooting-depth distributions with increased woody cover are likely to result in notable changes in soil hydrologic fluxes and flow paths (Beven and Germann 2013) with implications for vertical and lateral hydrologic connectivity in the subsurface (Banwart et al. 2019; Xiao, Brantley, and Li 2021) and biogeochemical processes such as chemical weathering and carbon fluxes and export (Wen et al. 2021, 2022).

Our study tested the degree to which woody encroachment in tallgrass prairie can alter root abundance, soil physical structure and hydraulic properties and soil water flow during rain events. We examined how flow velocities changed under woody and grassy cover as a function of antecedent soil water content and storm characteristics (duration and intensity), which other studies identify as important drivers of preferential flow (Hardie et al. 2013; Nimmo 2021). In addition to examining natural rain events, we also investigated soil wetting during a rainfall simulation using electrical resistivity (ER) tomography as a noninvasive way to understand the spatiotemporal distribution of infiltration dynamics during high rainfall intensity (e.g., Garré et al. 2011; Nimmo et al. 2009). We chose to examine soil water dynamics during intense rainfall because rainfall variability and intensity are expected to increase in many grassland systems as a result of climate change (Reidmiller et al. 2017). We hypothesised that the relatively coarse roots of woody shrubs would lead to deeper soil water infiltration and greater soil water flow velocities than the generally finer roots of grassland herbaceous species. We also hypothesised that high rainfall intensity would increase water movement to deeper portions of the soil profile beneath woody shrubs and grasses. However, we expected that the soil water flow velocities would be higher beneath shrubs than grasses across the range of rainfall intensities due to a greater abundance of coarse roots. The rapid response time in groundwater levels at the Konza Prairie also suggests that preferential flow is prevalent in the vadose zone (Vero et al. 2017). Thus, we do not expect infiltration excess to occur at our sites even when soils are near saturation. The propensity for preferential flow of water to deeper soil layers during high intensity rainfall may indeed benefit deeply rooted woody plants. For example, previous studies indicated that high rainfall intensity may increase the availability of deep soil water for woody-plant growth (Berry and Kulmatiski 2017; Holdrege, Beard, and Kulmatiski 2021; Kulmatiski and Beard 2013), although this effect is mediated by soil characteristics (Case and Staver 2018). We discuss the implications of our results for quantifying shifts in hydrologic connectivity and what such shifts can mean for critical zone functions.

2 | Methods

To investigate the role of woody encroachment in infiltration and drainage dynamics, we collected a combination of soil and

hydrological data from a mesic grassland. We examined the depth distributions of coarse and fine roots and soil hydraulic properties beneath grasses and beneath woody shrubs. Data describing soil properties provided important context for understanding the impact of woody encroachment on soil water flow. We calculated soil water velocities based on 2 years of rainfall and soil moisture data. In addition, we investigated the spatial and temporal disparities of soil water beneath woody and grass cover during a short-term rainfall simulation using ER imaging.

2.1 | Study Site

Our study took place in native tallgrass prairie at the Konza Prairie Biological Station in northeastern Kansas, USA (Figure 1a). The Konza Prairie is 3487 ha catchment divided into 60 subcatchments that are managed with different prescribed fire frequency (burned every 1, 2, 4 or 20 years) and grazing treatments (grazed by cattle, bison or ungrazed). The vegetation at the Konza Prairie includes dominant perennial C_4 grasses and a wide variety of C_3 grasses, forbs, and woody species. Roughleaf dogwood (*Cornus drumundii*) is the predominant woody shrub, showing rapid expansion in mesic tallgrass prairie since 2000 with a greater degree of woody cover in catchments that are burned less frequently (Ratajczak, Nippert, and Ocheltree 2014).

The climate is midcontinental with cool, dry winters and warm, wet summers. The mean annual water-year precipitation (1984–2022) was 838 mm, with most precipitation occurring as rainfall between April and September. The mean annual temperature from 1983 to 2023 was 12.9°C. July is the warmest month on average, with a mean temperature of 26.1°C between 1983 and 2023. January is the coldest month with a mean historic temperature of −1.1°C between 1983 and 2023 (Nippert 2024).

In this study, we leveraged existing data from two catchments that were burned at different frequencies resulting in high versus low woody-plant cover (Figure 1b). Catchment N4D (39.087356 N 96.584417 W) was burned every 4 years, and catchment N1B (39.08656 N, 96.57703 W) was burned annually since 1988. Both catchments are grazed by native bison and include diverse assemblages of grass and forb species. However, N4D has lower vegetation diversity and more woody cover than N1B as observed from 1-m resolution imagery from the USDA National Agriculture Imagery Program (US Department of Agriculture 2023; Figure 1b,c). We refer to our sites within N4D as 'woody-encroached' or 'shrub' and sites within N1B as 'grass'.

The bedrock at the Konza Prairie is merokarst and consists of limestone units interbedded between thicker mudstone units that create complex subsurface features including sinkholes and perched aquifers (Macpherson 1996; Sullivan et al. 2020). The limestone units at the Konza Prairie create high-relief bench and slope features with ~60 m of elevation change between the ridgetops and catchment outlets (Sullivan et al. 2019). Soils along the ridgetops are shallow loess (< 20–50 cm deep), while soils in the valley can reach up to ~2 m thick as a result of colluvial inputs from upslope (Hirmas and Mandel 2017; Johnson, Willey, and Macpherson 2007). Soil moisture profiles occur at three hillslope positions—summit,

backslope and toeslope—in each of the two study catchments (Figure 1c). The summit positions in the grass (N1B) and woody-encroached (N4D) catchment are in the Benfield–Florence complex, while the backslope positions are in the Clime-Sogn complex (Soil Survey Staff n.d.). The toeslope is within the Ivan and the Clime-Sogn complex in the grass catchment. In the woody-encroached catchment, the toeslope is within the Ivan map unit. The Benfield is classified as fine, mixed, superactive, mesic Udertic Argiustolls. The Florence is classified as clayey-skeletal, smectitic, mesic Udic Argiustolls. The Clime is classified as fine, mixed, active, mesic Udorthentic Haplustolls. The Sogn is classified as clayey, mixed, superactive and mesic Lithic Haplustolls, and the Ivan is classified as fine-silty, mixed, superactive and mesic Cumulic Hapludolls.

2.2 | Photo-Derived Root Abundance

As noted above, soil-monitoring sites were located at three hillslope locations—the summit, backslope and toeslope (Figure 1c). We define the summit as the relatively flat crest of the hill, the backslope as the mid or transition position between the upper and lower parts of the hill and the toeslope as the base of the hill. Soil pits in the woody-encroached sites were dug directly under roughleaf dogwood (*Cornus drummondii*), while pits in the grass sites were dug in grass-dominated areas where we could avoid forbs to the best extent possible. We removed soil up to 1 m below the surface. However, large rocky areas were encountered below 70 cm at the backslope and summit woody-encroached sites, which prevented us from digging to 1 m at all sites. After opening the soil pits, a vertical face was cleaned to expose undisturbed soil and roots. We photographed the vertical face of the soil pit from the surface down to a depth of 1 m, ensuring that the horizontal surface area captured was at least 20 cm wide.

The high-resolution photos (e.g., Figure S1) of the pit face were analysed in Image-J software (Schneider, Rasband, and Eliceiri 2012) to identify the presence (or absence) of fine and coarse roots. We used the software to overlay a 1×1 cm grid on each image. The grid was positioned to align with measuring tapes that spanned ~20 cm horizontally and up to 1 m vertically. The measuring tapes allowed the software to display grid cells with a known area. We recorded the presence of fine roots (diameter < 1 mm) or coarse roots (diameter > 1 mm) in each $1 cm^2$ grid cell. We focused on the presence/absence of roots in each cell, not the root count. If a cell had both fine and coarse roots, we only recorded the presence of coarse roots due to their larger volume, following methods in Billings et al. (2018). This approach was used based on each coarse root occupying a greater volume than a fine root and thus modifying soil structure to a greater extent. The presence/absence data at the centimetre scale were then converted into the fraction of each 5-cm-thick layer containing fine or coarse roots:

$$\text{Root fraction} = \frac{\sum \text{cells with presence of roots}}{\sum \text{total cells analysed}}.$$

We tested whether the distribution of root fractions from 10 to 70 cm differed beneath grass and woody shrubs. Root fractions for depths less than 10 cm were excluded from the analysis due
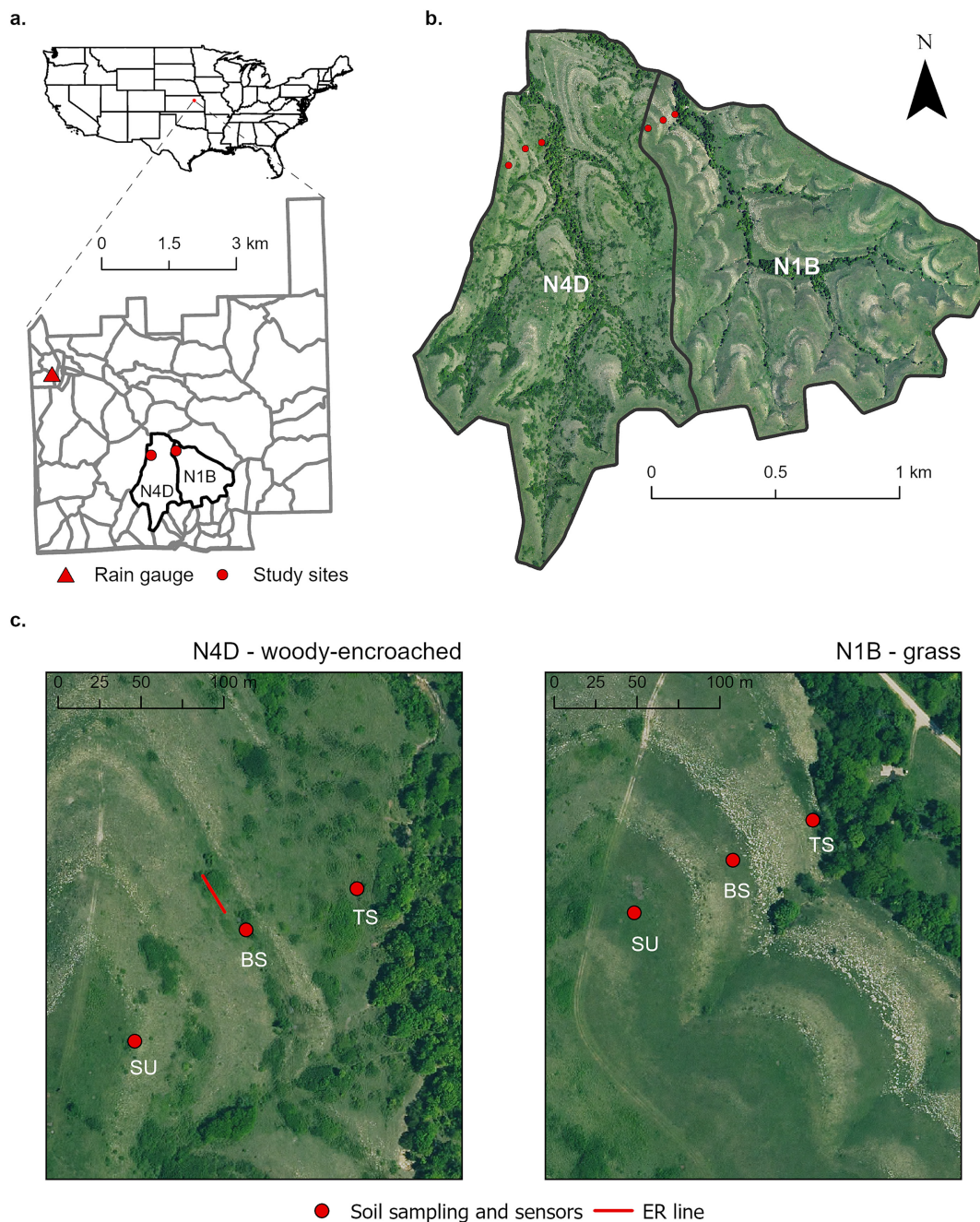
FIGURE 1 | (a) Location of the 3487-ha Konza Prairie Biological Station in northeast Kansas, USA. (b) The areal imagery shows the vegetation cover in our study watersheds, N4D and N1B. The woody-encroached watershed, N4D, is burned every 4 years, and the grass watershed, N1B, is burned annually, resulting in less woody shrub cover in upland areas. Riparian corridors include trees while upland areas are occupied by grasses, forbs and woody shrubs. (c) Soils were sampled for root abundance and soil physical properties at three hillslope positions—the summit (SU), backslope (BS) and toeslope (TS). Soil sensors at the backslope site in the grass and woody-encroached watersheds were used to assess soil water velocity during storm events. Electrical resistivity (red line) was measured beneath shrubs and grasses at the backslope site in the woody-encroached watershed.

to poor image quality; root fractions for depths greater than 70 cm were excluded because that was the deepest depth we could photograph across all soil pits. The root fractions were not normally distributed for each group, so we used a Mann–Whitney *U*-test to test for significant differences in median root fractions assuming a significance level of 0.05. This test was performed separately for each of the root classes—fine, coarse and total (proportion of fine or coarse roots).

2.3 | Soil Properties

We determined soil–water retention and saturated hydraulic conductivity (K_{sat}) at the summit, backslope, and toeslope sites (Figure 1c) by collecting undisturbed soil cores in triplicate from the A horizon at 15 cm and from B horizons at 40 and 60 cm. In addition, we collected bulk soil samples at 15, 40 and 60 cm to assess soil texture. We were unable to extract three

cores at each depth of the summit and toeslope sites due to rocky soils. As a result, we analysed soil properties at the backslope sites only. We did not test for statistical differences in soil properties beneath grasses and shrubs due to our limited samples size ($n = 3$). However, the availability of soil moisture and electrical-resistivity data at the backslope site allowed us to use multiple lines of evidence to address our research objectives.

We measured K_{sat} based on Darcy's law using the falling-head technique (Klute and Dirksen 1986) with the KSAT benchtop instrument (METER, Pullman, WA, USA). This instrument estimates K_{sat} for the bulk soil. Although macropores comprise small fractions of soil volume, they can contribute to more than 70% of soil water flow (Watson and Luxmoore 1986; Zhang et al. 2019). To explore the impact of soil macropores on soil water flow, we used the soil–water retention curve to estimate soil effective porosity as an indicator of soil macropores. We defined soil effective porosity from the perspective of the soil pore size distribution derived from the soil–water retention curve (Han, Giménez, and Lilly 2008). We estimated a unique inflection point (Figure S2) to distinguish the macropore and micropore domain for individual soil samples (Baver 1939; Dexter and Bird 2001).

Soil–water retention curves were derived from the soil cores used for K_{sat} measurements. We followed the evaporation method (Wind 1968) using a HYPROP system (METER, Pullman, WA, USA). In this study, we used soil–water retention data in the wet range, defined as matric potential > -1000 cm. The measured matric potential (h) and volumetric water content (θ) were fitted to the van Genuchten (van Genuchten 1980) water retention equation by optimizing θs, θ_r, α and n:

$$\theta = \theta_r + \frac{\theta_s - \theta_r}{\left[1 + (\alpha|h|)^n\right]^{1 - \frac{1}{n}}}$$

where θ_r (cm^{3}cm^{-3}) is the residual soil water content, θ_s (cm^{3}cm^{-3}) is the saturated soil water content, h (cm) is soil matric potential, α (cm^{-1}) is related to the inverse of the air-entry pressure head and n (dimensionless) is an empirical shape parameter. The inflection point occurs where the shape of the soil–water retention function transitions from convex to concave. The second derivative of the van Genuchten function with respect to h reflects changes in the curvature of the soil–water retention curve, which is influenced by the soil properties. The inflection point is the point at which the second derivative is zero (Dexter 2004). Therefore, the inflection point of each water retention curve can be identified by

$$h_i = \frac{1}{\alpha}\left(\frac{n}{n-1}\right)^{\frac{1}{n}}.$$

We defined effective porosity as the volume of soil water drained between saturation and the matric potential at the lower boundary of the macropore domain determined by the inflection point. The effective porosity (ϕ_{eff}) was then calculated as

$$\phi_{eff} = \theta_s - \theta\left(h_i\right).$$

The pore size distribution is unique across soils between sites (woody-encroached and grass) and among depths, resulting in distinct estimated porosity in the macropore domain using the

water retention curve in these locations. To separate nonequilibrium flow in macropores, we further calculated the matrix saturated hydraulic conductivity, which is controlled by soil texture (Lin et al. 1999). Matrix K_{sat} was estimated with the ROSETTA pedotransfer function using sand, silt and clay fractions; bulk density; and field capacity as inputs (Schaap, Leij, and Van Genuchten 2001). Thus, matrix K_{sat} represented the flow of water through largest fraction of water-filled pores of the soil matrix. We determined soil textural composition with the sieving and the pipette method (Gee and Or 2002). Soil bulk density was measured with the core method (Grossman and Reinsch 2002). Soil water content at a matric potential of -330 cm (-33 kPa) was calculated from the fitted van Genuchten water retention curve and was used as field capacity water content.

2.4 | Estimation of Soil Water Velocity

Soil moisture was recorded every 30 min from sensors (TEROS 12, METER, Pullman, WA, USA) that were installed horizontally into undisturbed soil at 15, 40 and 60 cm in November 2020. We used soil moisture and precipitation time series data between 1 April 2021 and 10 May 2023 (Figure 2) to estimate bulk soil water velocity during precipitation events > 2 mm. We excluded data between 10 May 2023 and 21 August 2023 due to missing data at the grass site that occurred due to a loss of power to the data logger. The remaining data did not contain missing values before 10 May 2023. We visually inspected the soil moisture and precipitation data for spurious data and outliers and concluded that the data did not require additional correction. Precipitation was assumed to infiltrate and flow vertically to reach soil sensors buried along a vertical soil profile. Thus, bulk soil water velocity was calculated as distance/time where distance was equal to the depth of the soil sensor (i.e., the distance of water flow through the soil profile from the land surface). Precipitation has been measured every 15 min since 2010 with an OTT Pluvio^2 rain gauge (OTT HydroMet) at the Konza Prairie Headquarters, located ~3 km from our study sites (Figure 1a). The backslope position had a complete record of half-hourly soil moisture data, whereas sites at toeslope and summit positions had extensive periods of missing data due to sensor or data logger malfunction. Thus, we performed the velocity analysis using only the soil moisture record from the backslope position.

We leveraged a method developed by Hirmas et al. (In review) to estimate the bulk soil water velocity using soil moisture time-series data. The method identified soil moisture peaks through a series of steps to evaluate outliers of the time derivative of the soil water content. First, a Hampel filter was used to detect outliers among the positive derivative values of the time-series data based on the median absolute deviation (MAD). Values greater than 3 MAD above the MAD were considered meaningful outliers and were retained as potential peaks. Next, the derivative values in log space were further filtered to include only peak values that were more than 1.5 times the standard deviation of the log derivative median. When soil moisture peaks were clustered within 2 h, the largest peak among the cluster of peaks was selected as the final peak for further analysis. Once the final soil moisture peaks were identified, the onset of each peak's rising limb was identified as an increase in soil moisture that exceeded 0.02 m^{3}m^{-3} and occurred between the soil moisture peak and the previous soil moisture
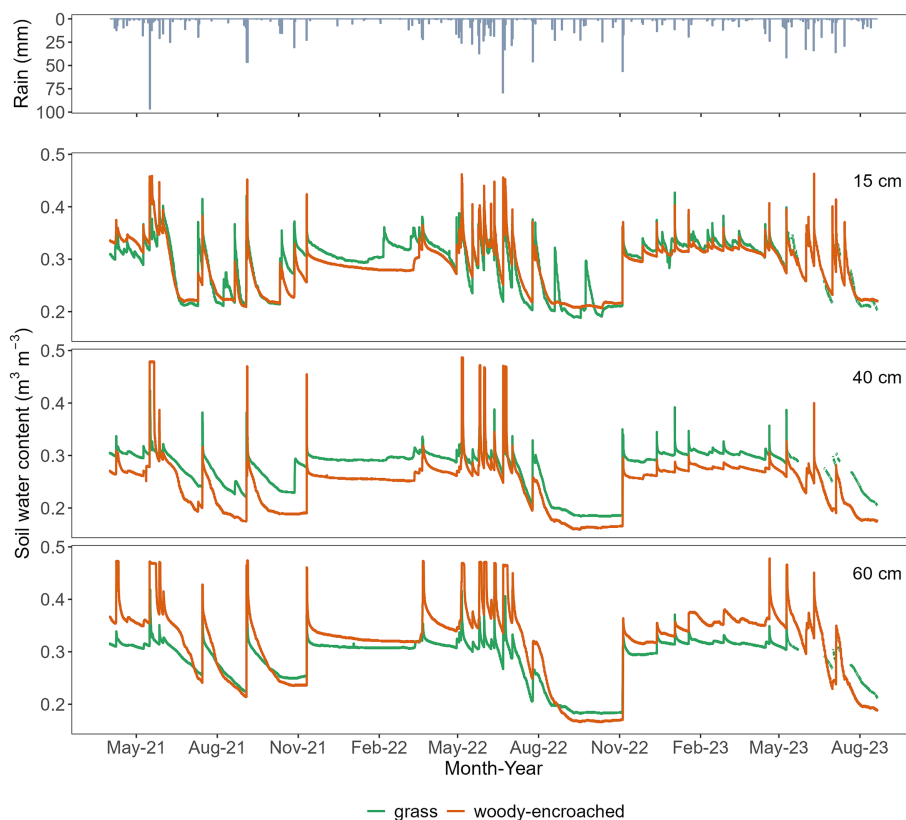
FIGURE 2 | Daily rainfall from the Konza Prairie headquarters and the soil moisture measured every 30 min from 1 April 2021 to 21 August 2023 at 15, 40 and 60 cm at the grass and woody-encroached backslope site. Soil water flow velocities (cm h^{-1}) were estimated using the onset time of the soil moisture rising limb ($n = 61$ for grass site; $n = 56$ for woody-encroached site) that occurred within 48 h of the storm onset.

peak. The soil moisture "event" was omitted if any missing values were present within a 2-h interval around the onset or peak time.

We used the precipitation-event delineation method used by Araki et al. (2022). The onset of a storm event was determined from nonzero precipitation measurements. Precipitation measurements nested within a 6-h period were classified as the same storm event. A threshold of 5 days was enforced as the maximum duration of an event to avoid excessively long events. Next, we assigned a unique identifier to each storm onset and soil moisture onset pair. We selected storm onsets that occurred within 2 days prior to the onset of the soil moisture peak event. Note that we removed an event from the analysis if the onset of the storm occurred more than 2 days before the onset of the soil moisture rising limb or if the onset of the storm followed the onset of the soil moisture rising limb due to relatively large distance between the meteorological station and our sites (Figure 1a). The bulk soil water velocity (cm day^{-1}) was calculated by the sensor depth (15, 40 or 60 cm) divided by the time difference between the onset of the storm and onset of the soil moisture rising limb. This value represented the fastest measurable component of water flow through the bulk soil. To account for the portion of water that would flow through the macropore domain of the soil, we multiplied the bulk soil water velocity by the effective porosity at each sensor depth. This normalised velocity value was referred to as the effective velocity (cm day^{-1}). The log-scaled effective velocities were approximately normally distributed. We compared the mean of log-scaled effective velocities at the grass and woody-encroached sites using an independent t-test and compared the variance using the F-test. We performed a linear regression to test how effective velocity was correlated to rainfall intensity, storm duration and antecedent soil water content. The storm duration was defined as the time span between the storm end and storm onset. The rainfall intensity was defined as the maximum rate of precipitation observation during a storm event. The antecedent soil water content was defined as the soil water content recorded 1 h before the storm onset time. Statistical analysis and visualisation were performed with R (R Core Team 2023).

2.5 | ER Imaging During Rainfall Simulation

We conducted a rainfall simulation from 23 to 24 August 2023 to test the spatiotemporal dynamics of soil water infiltration and drainage beneath grass and shrubs. Two plots were established in the woody-encroached watershed ~5 m upslope of the backslope site (Figure 1c). Each plot was 9 m^2, and plots were positioned ~8 m apart. One plot included grasses—big bluestem (*Andropogon gerardii*), switchgrass (*Sorghastrum nutans*) and Indiangrass (*Panicum virgatum*) as well as forbs—ironweed (*Vernonia baldwinii*), white sagebrush, (*Artemisia ludoviciana*), Canada goldenrod (*Solidago canadensis*) and butterfly milkweed (*Asclepias tuberosa*), and the other plot was dominated by roughleaf dogwood (*C. drummondii*).

A 24.5-m-long transect that passed through each plot was established for ER imaging. The centre of the grass plot was at

7 m along the transect, and the centre of the shrub plot was at 16.5 m along the transect (Figure 3a). The midpoint of the transect marked the transition from predominantly grass to predominantly shrub. The shrub *C. drummondii* is clonal and primarily spreads vegetatively to form large amorphous shrub 'islands' that buffer interior stems against fire (Nippert et al. 2021). Our shrub plot was located near the centre of a large shrub island. The stems of shrub *C. drummondii* in the centre of an island are generally the oldest, evident by greater height and stem diameter compared to the smaller stems on the periphery of an island. The transect was also positioned along an elevation isoline to avoid topographic effects of both the rainfall simulation and the ER measurements. We installed 48 electrodes spaced every 0.5 m along the transect and monitored soil ER using a Syscal Pro resistivity metre (IRIS Instruments, France). We used a dipole–dipole configuration with 735 quadripoles. Each quadripole was stacked three to five times for QA/QC, and the standard deviation of the stacked measurements was used to weight the data during inversion. ER acquisition took place during five data acquisition periods from 22 to 24 August, during which multiple ER surveys were automatically collected approximately every 30 min, resulting in 40 total data sets (Figure 3b). We collected three data sets (Period 1) on 22 August to map natural variability prior to the rainfall simulation. Periods 2, 3 and 4 took place before, during and after each of three rain pulses from 23 to 24 August, and the final collection period (Period 5) took place before dismantling the setup on 24 August (Figure 3b).

We used two sprinklers with an oscillating motor attached to a tripod base to deliver water to each of the two plots. More information on the sprinkler system can be found in Dodds et al. (2022). The tripod was positioned in the centre of the plot and directly above the ER transect. Water was delivered as three 'rain' pulses spaced 12 h apart. To observe soil moisture changes in the upper 2 m of soil, we chose to apply a volume of water that was representative of the largest storm events observed at the Konza Prairie between 2001 and 2022. Each pulse delivered ~850 L of water or an equivalent of ~5 cm of rainfall to each plot, resulting in a total of ~15 cm of rainfall over the three pulses. This total fell within the upper range of the long-term (2001 to 2022) maximum weekly rainfall observed at the Konza Prairie during the growing season. The 95th percentile of weekly total rainfall was 8.4 cm, and the maximum weekly total was 17.6 cm. Although the same amount of water was distributed onto the plot during each pulse, the rate of application was slightly different due to issues with the water pump during the first pulse. The initial pulse lasted ~60 min due to insufficient water pressure to the pump. This issue was resolved after the first pulse was complete. The second and third pulses each lasted ~35 min.

To account for changes in soil temperature in the near-surface soil environment, we corrected the apparent resistivity to a standard temperature of 25°C following the methods in Hayley et al. (2007). Soil temperature was measured every 30 min over the duration of the experiment using soil temperature sensors (TEROS 12, METER Environment) buried at three depths in the soil profile—15, 40 and 60 cm. We defined a pseudo depth for each quadripole following methods described in Edwards (1977). Apparent resistivity for pseudo depths 0–15, 15–40 and >40 cm was corrected using the temperature data at 15, 40 and 60 cm, respectively. Soil temperature ranged from 26.3°C to 27.7°C at 15 cm, 25°C to 25.3°C at 40 cm and 23.6°C to 23.8°C at 60 cm during the duration of the rainfall experiment (Figure 3b). We assumed that soil
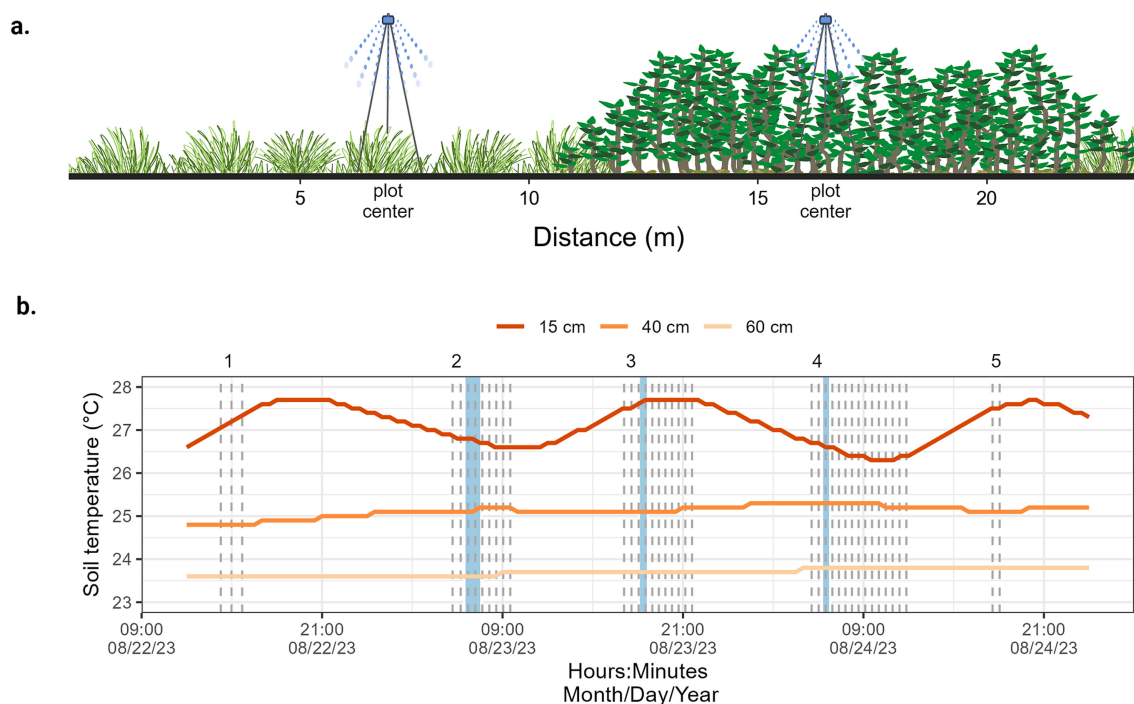

FIGURE 3 | (a) A schematic showing the position of grass and shrub plots along the 24.5 m electrical resistivity (ER) transect. (b) The median time of each ER data set is shown as dashed grey lines, and the start and end of the rain pulse is shown as blue boxes. Data sets were collected from 22 to 24 August 2023 during five distinct periods labelled at the top of the plot. Five background data sets were collected before the first rain pulse. All data were corrected for soil temperature.

temperature was laterally uniform and did not vary below 60 cm, the latter of which seemed reasonable given the measured temperature ranges.

Temperature-corrected data were inverted using ResIPy 3.4.5 (Blanchy et al. 2020). First, the prerainfall data were inverted separately to obtain five background resistivity profiles. We used the inverted prerainfall data sets to calculate the mean coefficient of variation induced by repeat ER measurements as an indicator of background variability. We estimated the background variability of the prerainfall data during Period 1 to be 4.6%, which led to changes of up to 18% in the inverted models. Only resistivity differences greater than this were considered meaningful. The prerainfall data set with the lowest mean stacking error the morning of the rainfall experiment was used as our background data set during difference inversion. We did not filter the ER data sets, and the stacking errors for each data set were used as the error model in the resistivity difference inversions. The median stacking error was 0.56%, and the mean stacking error was 1.7%. We used linear filtering to regularise the difference inversion for estimating change in resistivity (LaBrecque and Yang 2001). The final weighted root mean square error, normalised to the data error, varied between 1.1% and 2.4% with a mean of 1.6% (Table S1). In addition, we quantified the depth below which the data did not affect the inversion in the inverted background data sets using the depth of investigation method (Oldenburg and Li 1999). Inversions generally were sensitive to the top 2 m of the subsurface. A negative change in resistivity indicated a decrease in resistivity from the prerainfall data, which was used as a proxy for examining the spatial and temporal patterns of soil wetting. To further examine the temporal patterns of soil wetting, we estimated the average resistivity for multiple soil depths under the centre 2 m of the grass and shrub plot each. The centre of the plot was directly below the sprinkler (Figure 3a) and therefore received the most rainfall. The average resistivity values were estimated for each 10-cm depth increment up to 2 m, which were considered meaningful data based on the modelled depth of investigation.

3 | Results

3.1 | Soil Properties

Both the coarse and total root fractions from 10 to 70 cm were greater beneath shrubs than grasses ($p < 0.001$; Figure 4). In contrast, the fine root fraction from 10 to 70 cm did not differ beneath shrubs and grasses ($p = 0.92$). In general, root fraction decreased with increasing soil depth at both shrub and grass sites (Figure 4). Average coarse-root fraction was greater beneath shrubs than grasses across all soil depths. In contrast, average fine and total root fractions appeared to be greater beneath shrubs primarily between 35 and 50 cm.

We could only assess the saturated hydraulic conductivity and effective porosity at the backslope position due to difficulty extracting soil cores in rocky soils at the summit and toeslope. The soil texture at the grass backslope was silty clay loam at 15 and 60 cm and clay loam at 40 cm. The soil texture at the woody-encroached backslope was silty clay at 15 cm and clay at 40 and 60 cm. The mean and standard error of bulk and matrix K_{sat} for the grass and woody-encroached site were calculated from three replicate cores taken at each of three depths—15, 40 and 60 cm (Figure 5). The mean bulk K_{sat} across all depths was 68 cm h^{-1} at the woody-encroached site and 20 cm h^{-1} at the grass site. Although each set of replicate soil cores was extracted from the same soil pit, the inclusion of rock and root fragments led to highly variable bulk K_{sat}. The highest bulk K_{sat} beneath woody shrubs was in the B horizon at 60 cm (mean = 116 ± 75 cm h^{-1}). In contrast, bulk K_{sat} beneath grasses was highest in the A horizon at 15 cm (mean = 24 ± 15 cm h^{-1}). The effective porosity declined with depth beneath both vegetation types. However, soils
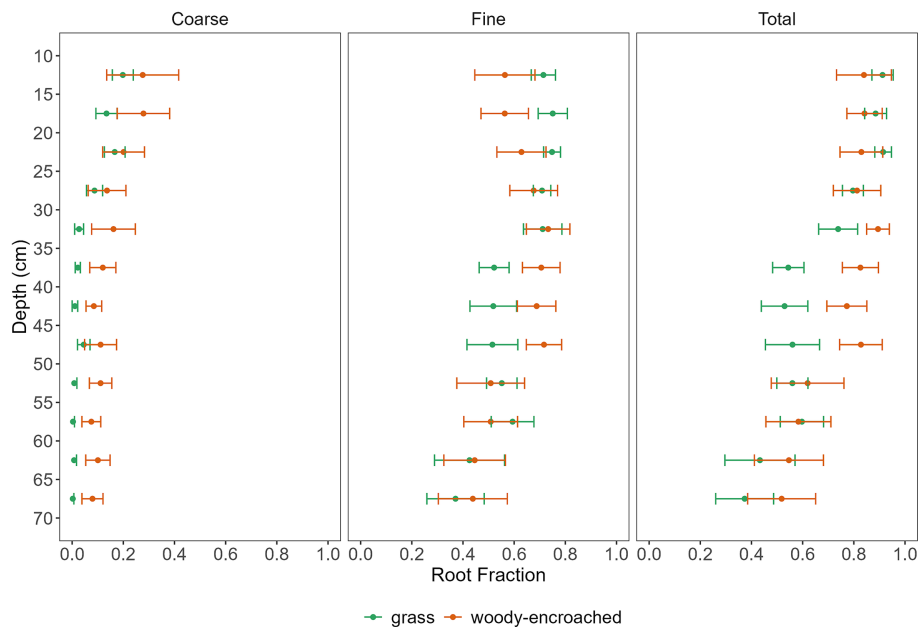

FIGURE 4 | We used high-resolution photos from six soil pits beneath grasses and woody shrubs to estimate the fraction of coarse, fine and total roots in each 5-cm depth interval. Data show the mean and standard error for each 5 cm increment between 10 and 70 cm.

beneath shrubs appeared to have a greater mean effective porosity than soils beneath grasses. This was most pronounced in the B horizon at 60 cm, with the mean effective porosity being $0.03\,m^3\,m^{-3}$ greater at the woody-encroached site compared to the grass site (Figure 5c). Additional details on soil properties are provided in Table S2.

3.2 | Soil Water Storage and Flow

We examined the distribution of soil water content measured half-hourly from 1 April 2021 to 10 May 2023 at the woody-encroached and grass backslope site. There were no missing values recorded within this time frame. The mean and distribution of soil water content at 15 cm were similar beneath grasses and shrubs but notably different at the deeper B horizon depths, 40 and 60 cm (Figure 6). The mean soil water content was $0.02\,m^3\,m^{-3}$ greater beneath grasses than shrubs at 40 cm. In contrast, the mean soil water content was $0.03\,m^3\,m^{-3}$ greater beneath shrubs than grasses at 60 cm (Table 1 and Figure 6). The woody-encroached site had a greater range in soil water content at 40 and 60 cm than the grass site. For example, the maximum soil water content at 40 and 60 cm was higher, and the minimum soil water content was lower beneath shrubs than grasses (Table 1).

The mean bulk soil water velocity was not statistically different between the grass and woody-encroached sites at any of the soil depths. When bulk soil water velocity was normalised by the effective porosity, we observed slightly greater mean effective velocities at the woody-encroached site than at the grass site in the B horizon at 40 and 60 cm (Figure 7). However, the difference in mean effective velocity between the grass and woody-encroached sites was not statistically significant at any of the depths. Note that we analysed the soil water velocities on a log scale due to the skewed distribution of the data. Bulk soil water velocity across all sites and depths ranged from 1 to $120\,cm\,h^{-1}$ with an overall mean equal to $14\,cm\,h^{-1}$, and the median bulk soil water velocity increased with depth at both the woody-encroached and grass sites (Figure S3). All values of bulk soil water velocity exceeded the matrix K_{sat} at 40 and 60 cm. The effective velocities were not well correlated to storm duration (data not shown). Antecedent water content and rainfall intensity appeared to be positively correlated with effective velocity beneath shrubs (Figure 8). The
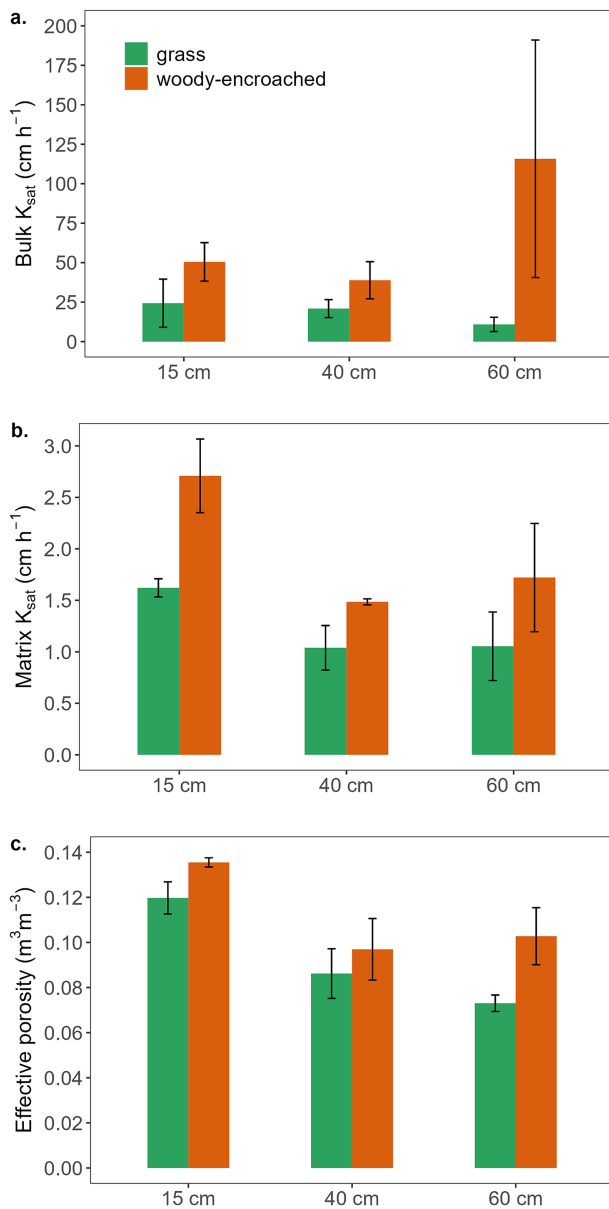

FIGURE 5 | (a) Bulk saturated hydraulic conductivity (K_{sat}), (b) matrix K_{sat}, and (c) effective porosity were measured from three cores taken as each sample depth—15, 40 and 60 cm—at the backslope site in the grass and woody-encroached watershed. The mean and standard error values of the three cores collected at each depth are shown.
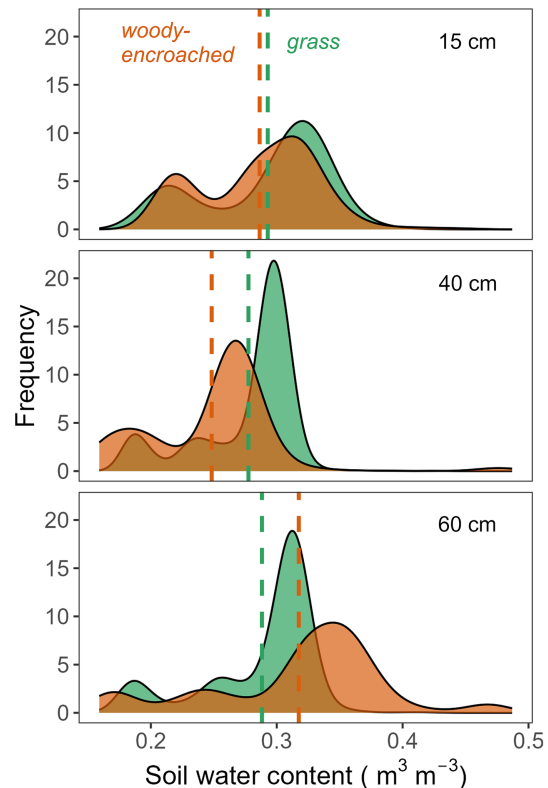

FIGURE 6 | The kernel density distribution of soil water content measured half-hourly at 15, 40 and 60 cm from 1 April 2021 to 10 May 2023. The dashed line indicates the mean soil water content value at the woody-encroached (orange) and grass (green) site.

TABLE 1 | The mean, maximum and minimum soil water content ($m^3 m^{-3}$) at 15, 40 and 60 cm at the grass and woody-encroached backslope site from half-hourly measurements between 1 April 2021 and 10 May 2023.

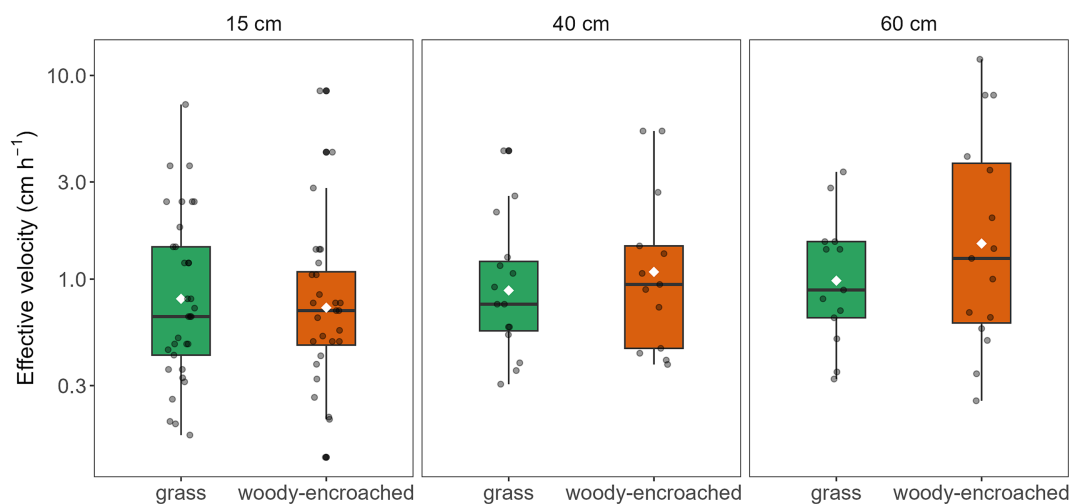| Site	Depth	Mean ($m^3 m^{-3}$)	Max ($m^3 m^{-3}$)	Min ($m^3 m^{-3}$)
Grass	15 cm	0.29	0.43	0.19
Grass	40 cm	0.28	0.42	0.18
Grass	60 cm	0.29	0.42	0.18
Woody-encroached	15 cm	0.29	0.46	0.21
Woody-encroached	40 cm	0.26	0.49	0.16
Woody-encroached	60 cm	0.32	0.48	0.17

FIGURE 7 | The effective velocity ($cm\,h^{-1}$) is shown on the log scale. The number of events for which the effective velocity was calculated was greater in the A horizon at 15 cm ($n = 33$ for grass and $n = 28$ for shrub) than in the B horizons (40 cm: $n = 15$ for grass and $n = 13$ for shrub; 60 cm: $n = 13$ for grass and $n = 15$ for shrub). The mean effective velocity (white diamond) increased with soil depth but was not statistically different between the grass and woody-encroached sites at 15 ($p = 0.67$), 40 ($p = 0.52$), or 60 cm ($p = 0.27$). Similarly, the variance of the effective velocities did not differ beneath shrubs and grasses at 15 ($p = 0.81$), 40 ($p = 0.50$) or 60 cm ($p = 0.08$).

log-scaled effective velocity showed a positive linear correlation with antecedent water content at the woody site ($p = 0.002$) but not at the grass site ($p = 0.4$). Similarly, log-scaled effective velocity at the woody-encroached site had a positive linear relation to log-scaled rainfall intensity ($p = 0.03$) but showed no relationship at the grass site ($p = 0.1$). Although the relationships between environmental variables and effective velocity were statistically significant at the woody-encroached site, the relationships were weak ($r^2 < 0.2$).

3.3 | ER During Rainfall Simulation

Water was applied to the shrub and grass plot in three pulses for a total of 15 cm of rainfall in ~36 h. We conducted the rainfall simulation in late August following an extended period of soil drying from mid-July to mid-August. Prior to the rainfall experiment, soil water content in the upper meter of soil was the lowest observed during the 2023 growing season (Figure 2). The spatial and temporal evolution of ER was examined as the percent

change in resistivity from background conditions. Decrease in resistivity during the rainfall simulation was used as a proxy for soil water increase.

We observed a notable decrease in resistivity in the upper 0.5 m within 2 h of the first rain pulse (Figure 9a). During the initial rain pulse, we also observed a larger decrease in resistivity for shallow soils beneath the shrubs than grasses (Figure 10). However, following the second and third rain pulses, we observed a similar decrease in resistivity in the upper 0.5 m beneath both vegetation types. In contrast, we observed a different response beneath shrubs and grasses between 0.5 and 2 m. At depths below 0.5 m, we found little to no detectable change in resistivity beneath the grasses (Figure 10a) and relatively minor (< 20%) decreases in resistivity beneath the shrubs (Figure 10b) during the first rain pulse. However, after the second rain pulse, the decline in resistivity was spatially variable from 0.5 to 1 m beneath the grasses, while there was a notable decrease in resistivity (20% to 60%) from 0.5 to 1 m beneath the shrubs. In addition, we observed a greater degree of lateral wetting in the top meter of soil beneath the grasses
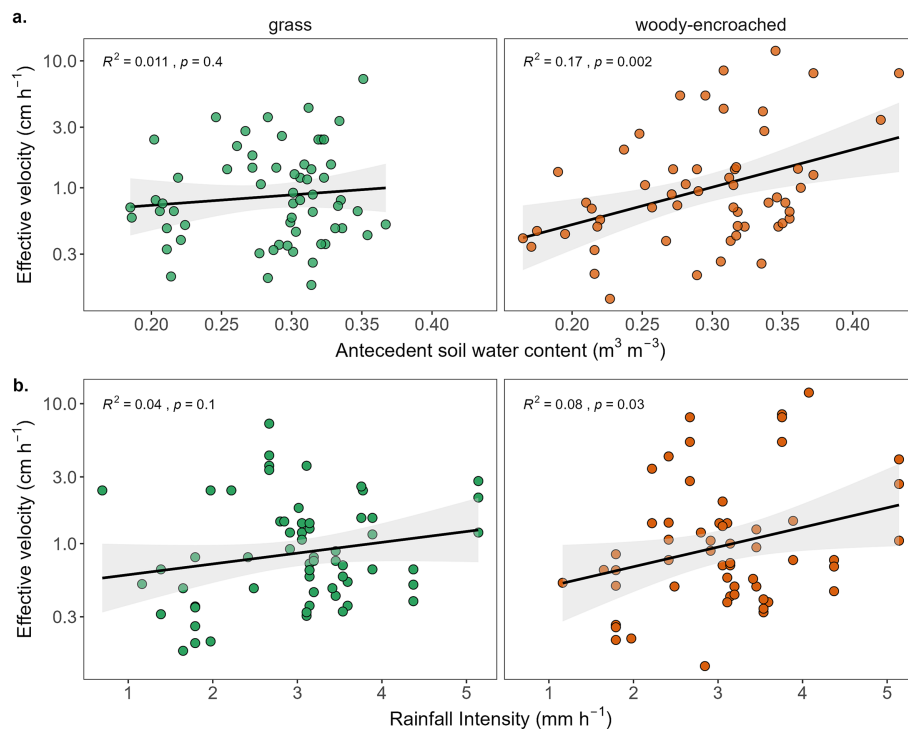
FIGURE 8 | (a) Effective velocity on the log scale had a positive linear correlation with the antecedent soil water content at the woody-encroached site ($p = 0.002$) but not at the grass site ($p = 0.4$). (b) Log-scaled effective velocity also had a weak, positive linear correlation to log-scaled rainfall intensity at the woody-encroached site ($p = 0.03$) while no significant correlation was observed at the grass site ($p = 0.1$). Grey band is the 95% confidence interval for the regression line.

than beneath the shrubs after the second and third rain pulses (Figure 9b,c). After the third and final rain pulses, resistivity decreased by more than 20% up to 2-m depth beneath the shrubs; a similar magnitude of change in resistivity was restricted to 1 m beneath the grasses (Figures 9c and 10). The final measurements were collected ~36 h after the start of the first rain pulse. At this time, resistivity had decreased between 38% and 80% in the top 2 m of profile beneath the shrubs, while the decrease in resistivity beneath the grasses ranged from 20% to 82% and was confined to the top 1.2 m.

4 | Discussion

Our study compared how woody encroachment-impacted changes in root abundance, soil hydraulic properties and soil water flow compared to the native grassy state. The abundance of coarse roots was greater beneath shrubs than grasses, which may have increased preferential flow of water to deeper depths below shrubs. Moreover, the differences in infiltration observed beneath these two vegetation types may also be the result of concentrated water delivery via stem flow below the woody shrub canopy. Saturated hydraulic conductivity (K_{sat}) and effective porosity were also greater below shrubs than grasses suggesting that shrubs also affect soil hydraulic properties in ways that may result in deeper flow paths and faster flow velocities, potentially altering vertical hydrologic connectivity in woody-encroached grasslands. These findings support previous modelling results that predicted a greater contribution of deep flow paths to streamflow generation following woody encroachment at the Konza Prairie

(Sadayappan et al. 2023). In addition, our work highlights the importance of future studies exploring how soil properties are influenced by altered rooting architectures in ways that drive modified soil water flows. Below, we discuss potential mechanisms that led to our observations, including preferential flow along live and/or dead root channels, and increased soil macropores via root growth and decay.

4.1 | Faster and Deeper Water Flow Beneath Shrubs Than Grasses

During the rainfall simulation, notable decreases in ER were observed up to 1 m beneath grasses and up to 2 m beneath shrubs, suggesting that more water moved to deeper soil layers beneath shrubs than grasses. In contrast, there appeared to be a greater degree of lateral wetting underneath grasses than shrubs. Deeper water flows beneath shrubs may be attributed, in part, to root-induced preferential flow that moved water to deeper soil layers while bypassing a portion of the soil matrix. Woody shrubs are associated with deeper rooting systems and a greater proportion of coarse roots compared to grasses (Figure 4). We found that, on average, the fraction of coarse roots for each 1-cm depth increment ER between 10 and 70 cm depth was 2.5 times greater beneath shrubs than grasses.

Previous work has shown that root size and density play important roles in promoting preferential flow along live roots as well as dead root channels, which can facilitate deep soil water recharge. For example, the flow of water along the
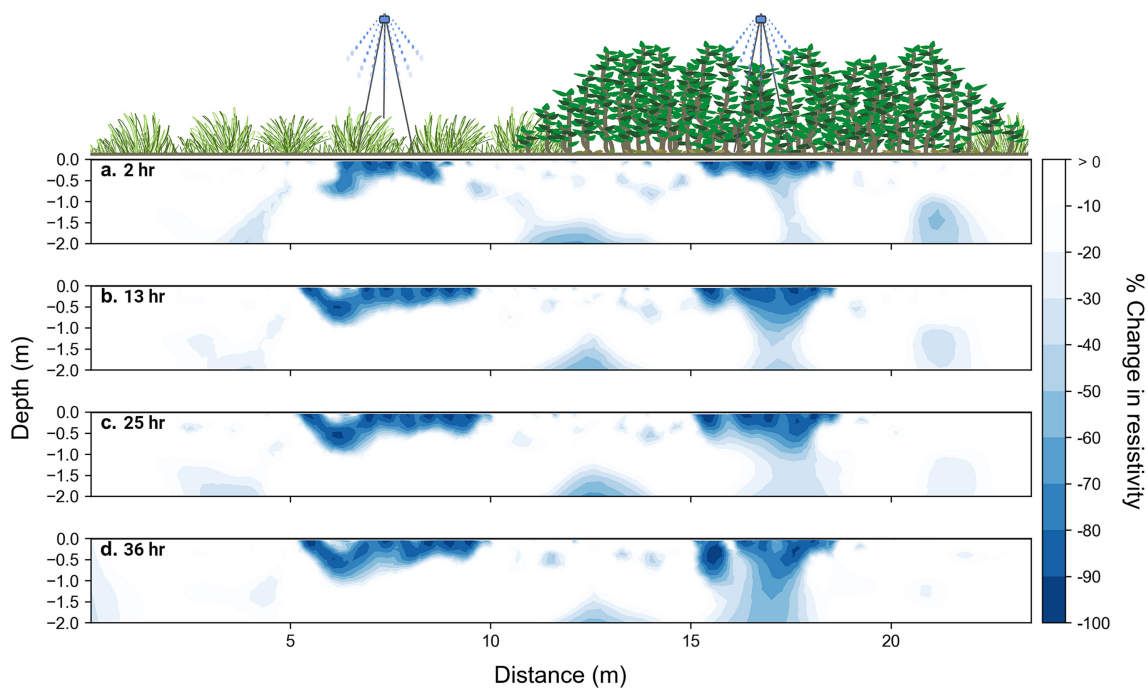
FIGURE 9 | Percent change in electrical-resistivity data during a three-pulse rainfall simulation from 23 to 24 August 2023. The grass and shrub plot received 5 cm of water during each pulse separated by 12 h. Time since the start of the first rain pulse is displayed on the left. Images in panels a, b and c were collected within 2 h after the first, second and third rain pulses, and panel d displays the final measurements 36 h after the first rain pulse. Decreases in resistivity are shown in blue and indicate an increase in subsurface water content. Positive percent change (increases in resistivity) or a negative percent change within the background variability (0% to −18%) is shown as white in the image since these data likely represent artefacts in the inversion process.

soil-root interface, known as funnel flow, has been observed where there is a relatively high root density in forest soils (Bogner et al. 2010). Also, coarse roots, such as tap roots, of trees can facilitate soil water recharge up to 2.7 m (Burgess et al. 2001). Moreover, decayed roots of woody shrubs can enhance the downward movement of water to deeper depths in arid environments (Devitt and Smith 2002).

In addition to funnel flow, the deeper and faster water flow beneath shrubs may be explained by root effects on soil porosity and hydraulic properties. We found greater effective soil porosity and saturated hydraulic conductivity beneath shrubs than grasses. This finding aligns with previous studies that found coarse roots, in general, increased K_{sat}, especially in fine-textured soils (Lu et al. 2020). It is possible that an increase in coarse-root abundance beneath shrubs led to the observed increase in effective porosity. Root channels, formed by live, dead, or decaying roots, are considered biotic macropores. Water tends to flow more quickly and efficiently through soil macropores compared to the smaller pores found within the soil matrix. Small increases in effective porosity can increase K_{sat} exponentially because Poiseuille's law states that the flow rate in fluid-filled pores is proportional to the fourth power of the pore radius. Moreover, controlled experiments on intact soil columns indicate that macroporosity and the number of independent macropore paths can explain up to 75% of the variability in K_{sat} values (Luo, Lin, and Schmidt 2010).

We expected that differences in effective porosity at the grass and woody-encroached sites would also lead to differences in

soil water velocities. We found greater mean effective velocity (bulk soil water velocity normalised by the effective porosity) beneath shrubs than grasses (Figure 7), which may indicate that an increase in macropores at 40 and 60 cm elevated effective velocities beneath shrubs compared to grasses. However, the effective velocities beneath shrubs and grasses were also highly variable among storm events. As a result, the difference in mean effective velocity beneath shrubs and grasses was not statistically significant at any measured depth. This may be attributed, in part, to a relatively small number of events that could be used to quantify bulk soil water velocity. Although there were 90 storm events with more than 2 mm of rainfall during our 2-year analysis period, we were only able to calculate soil water velocities at 15 cm for 42% of the storm events and at 40 and 60 cm for 18% and 19% of storm events. While not every storm event initiated a notable soil moisture increase, there were other factors that limited our ability to calculate soil water velocities for more storms. First, soil moisture was recorded every 30 min, making it difficult to accurately estimate the timing of the soil moisture peak onset since soil moisture can increase over the span of minutes. Second, rainfall was recorded 3 km from our soil moisture monitoring sites (Figure 1a). The relatively coarse temporal resolution of soil moisture data and the large distance between rainfall and soil moisture sensors can lead to uncertainties in the recorded time of the soil moisture peak and storm onsets. This was evident in our data set when the onset of the soil moisture rising limb preceded the storm onset.

Another factor that can influence the infiltration and drainage dynamics of rainfall is canopy interception and stemflow.
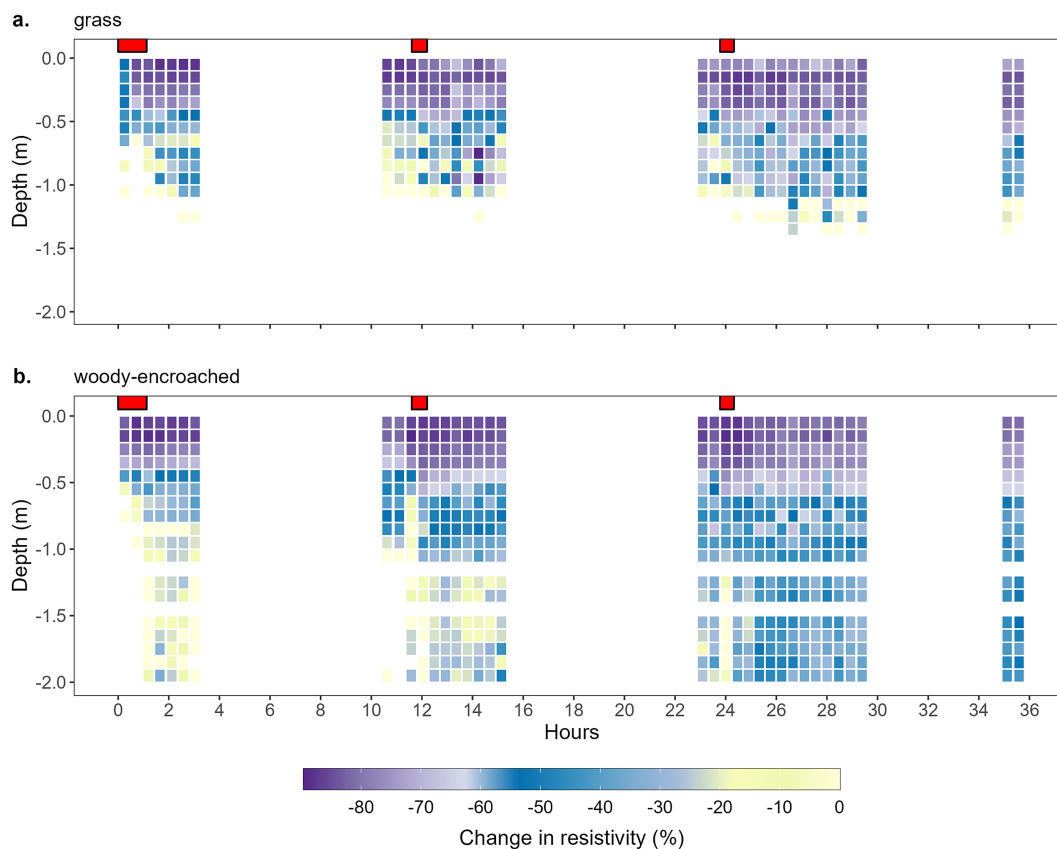
FIGURE 10 | The average percent change in resistivity over time for each 10-cm layer beneath (a) the centre of the grass plot and (b) the centre of the shrub plot. The median time stamp for each survey ($n = 35$) is displayed on the x-axis as hours since the start of the first rain pulse. Red blocks at the top of each plot indicate the start and end time of each of the three rain pulses. If the change in resistivity was positive, we chose not to display the data at this depth (e.g., white space) since these data likely represent artefacts of the inversion process. Yellow colours indicate no change because differences in resistivity from the background are within the range of the natural variability of our prerainfall measurements.

While we did not measure these processes in our study, we observed that the canopies of shrubs and grasses played an important role in the redistribution of water to the soil surface during the rainfall simulation. Anecdotally, we observed that a fraction of water was intercepted by the shrubs and rerouted via stemflow to the centre of the woody plot. In contrast, rainfall was more evenly distributed in the grass plot, resulting in a greater surface area that received water. While we do not have direct evidence of water flow along coarse roots at the base of the woody stems, it is possible that the concentration of water along the stem induced preferential flow along coarse roots, which led to an accumulation of water in deeper soil layers. The observation agrees with previous studies that conclude that a disproportionate amount of precipitation is funnelled to the base of shrubs and trees, creating preferential entry of water into the soil along root-channel macropores (Guo et al. 2020; Levia and Frost 2003; Li et al. 2009; Schwärzel, Ebermann, and Schalling 2012). Precipitation that has been channelled by leaves and branches and eventually flows down the stem can alter the chemical composition of water entering the soil due to dry deposition on leaves and foliar leaching into the rainwater (Johnson and Lehmann 2006). Thus, from an ecological perspective, the double-funnelling of water along stems and roots may be beneficial for woody plants because deeper nutrient fluxes would promote root growth over a greater soil volume.

4.2 | The Influence of Antecedent Moisture on Preferential Flow Beneath Shrubs and Grasses

Water flow in soil is typically categorised as uniform flow or preferential flow. The bulk soil water velocities observed following natural rainfall events provide evidence that preferential flow is common beneath both grasses and shrubs at our site (Figure S1). Bulk soil water velocity has been used in previous studies to identify the occurrence of preferential flow (Hardie et al. 2013). If velocities exceed the matrix K_{sat}, the infiltrated water is likely moving faster than diffuse flow of the wetting front. We found that, among all depths, the mean bulk soil water velocity was eight times greater than average matrix K_{sat} beneath the shrubs and 11 times greater beneath grasses. Thus, for the average storm event, infiltrated water appeared to be moving faster than diffuse flow in the soil matrix, indicating the occurrence of preferential flow beneath both grasses and shrubs. While we were not able to calculate the volume of water moving to depth, the greater effective velocities (bulk soil water velocity normalised by the effective porosity) below shrubs than grasses indicated that shrubs have the potential to expedite water flow through macropores. In addition, we found that, where shrubs were present, a relation emerged between effective velocities and factors that are known to influence the occurrence of preferential flow—antecedent water content and rainfall intensity. We found that effective velocities were greater under wetter antecedent conditions below shrubs. However, this was not

the case for soil water velocities below grasses (Figure 8). Thus, storm events that occur during relatively wet antecedent conditions below shrubs may be more likely to induce preferential flow and move water to deeper soil depths. This is also corroborated by our observations that deeper (> 1 m) drainage beneath the shrubs during the rainfall simulation occurred only after shallow soils became wet during the first rain pulse (Figure 9b). Preferential flow generally manifests after soils have reached a threshold antecedent water content, with macropores becoming hydraulically active (Nimmo 2021). However, research findings vary regarding how antecedent moisture levels affect soil water flow. Some studies find a greater occurrence of preferential flow with higher antecedent water content (Hu et al. 2019), while others indicate a decrease in preferential flow (Hardie et al. 2011).

Another factor that has been shown to influence soil water velocities and the occurrence of preferential flow is rainfall intensity. Our findings align with previous studies that found a positive correlation between rainfall intensity and the occurrence of preferential flow (Hu et al. 2019; Wiekenkamp et al. 2016) and deeper soil water fluxes (Kulmatiski and Beard 2013). The simulated rainfall intensity during our ER measurements was ~96 mm h^{-1}. This represents an extreme event at the Konza Prairie where the 95th percentile of rainfall intensity observed from 2021 to 2023 was 70 mm h^{-1}, and the maximum was 171 mm h^{-1}. The relatively high rainfall intensity during the rainfall simulation may have contributed to the deep infiltration of water (below 1 m) in the shrub plot. It is possible that the depth of infiltration may have been shallower with a lower rainfall intensity. Moreover, the antecedent soil moisture condition prior to the rainfall simulation was relatively dry. Thus, simulating rainfall during three separate periods over 2 days allowed us to increase antecedent soil moisture by the third rain pulse, which is when we observed the deepest penetration of water in both plots (Figure 10).

At the Konza Prairie, soils are wetter from October to March when vegetation is dormant compared to the growing season (April to September). Thus, we might expect storm events during this period to contribute a greater proportion of incident precipitation to deeper depths. Previous work at the Konza Prairie concluded that increased soil infiltrability beneath shrubs may reduce soil water residence times (Anhold 2023) and increase the movement of water to greater depths (Keen et al. 2024). However, while deeper drainage may occur in the dormant season, woody encroachment may also reduce total recharge on an annual basis due to elevated transpiration rates of woody shrubs compared to grasses during the growing season (Keen et al. 2022; O'Keefe et al. 2020). A decline in recharge has also been observed in a drier climate setting of a subhumid prairie where deeper soil drying beneath encroaching eastern red cedar compared to grasses reduced the overall downward flux of water below 2 m (Acharya et al. 2017). Thus, the impact of antecedent moisture on preferential flow and vertical hydrologic connectivity may depend on seasonality, climatic setting and subsurface hydraulic properties.

4.3 | Implications for Hydrologic Connectivity and Catchment Coevolution

The net effects of woody encroachment—and associated root systems—on groundwater recharge and streamflow are not well

understood across diverse systems. Increases in woody cover—which alters both ET and soil infiltrability—may enhance or reduce hydrologic connectivity depending on climate, plant physiology, soils and bedrock composition (Wilcox et al. 2022). In arid rangelands, woody shrubs and trees appear to promote vertical preferential flow and deeper water percolation than in intercanopy spaces (Bargués Tobella et al. 2014; Devitt and Smith 2002). Laterally oriented roots can also promote preferential flow (Ghestem, Sidle, and Stokes 2011). Root influences on soil infiltrability can impact hydrologic connectivity at larger scales. However, this phenomenon is rarely incorporated into hydrologic models. The effect of woody cover increase on soil infiltrability in our study aligns with conclusions drawn in relevant studies conducted in a diversity of conditions. The combination of geophysical, soil and root data used in our study provides a basis for calibrating hydrologic models to improve projections of the preferential-flow pathways that impact streamflow generation.

Another important implication of woody encroachment and enhanced vertical connectivity is how it can affect chemical weathering, stream-water chemistry and the evolution of catchment landforms over longer timescales than those addressed by our study (Wen et al. 2021, 2022; Xiao, Brantley, and Li 2021). Given the 'fill-and-spill' nature (Tromp-van Meerveld and McDonnell 2006) of the merokarst environment at the Konza Prairie (Hatley et al. 2023), the change in infiltration patterns and possible accompaniment of change in biogeochemical function with woody encroachment may create the ideal environment to study catchment coevolution, defined as 'the process of spatial and temporal interactions between water, energy, bedrock-derived minerals, sediments, carbon, ecosystems and anthropogenic influences that lead to changes of catchment characteristics and responses' (Troch et al. 2015). For example, Wen et al. (2021) demonstrated with numerical experiments that carbonate-weathering rates at the Konza Prairie can double due to enhanced water and carbon fluxes at deeper depths following woody encroachment. In addition, long-term stream-water chemistry data from a woody-encroached watershed at the Konza Prairie have shown an increase in chemical weathering (Macpherson and Sullivan 2019), while groundwater concentrations of CO_2 have also been rising (Macpherson 2009; Macpherson et al. 2019). These changes may be occurring because of woody encroachment. Moreover, average annual precipitation and temperature have both been increasing at the Konza Prairie over the past several decades (Keen et al. 2024; Sadayappan et al. 2023), and our data suggest changes in infiltration patterns with increased woody cover. These changes have the potential to stimulate generation of soil CO_2 (Vero et al. 2017) and increase the flux of CO_2 into the subsurface. Anhold (2023) found higher dissolved CO_2 concentrations in groundwater from the grassy watershed (N1B) compared to the woody-encroached watershed (N4D) and suggested that the difference may reflect decreased soil water residence time in response to woody encroachment. Specifically, if soil water-residence time is lower in the woody-encroached watershed, then it would decrease the time available for open-system weathering in the soil, leading to greater drawdown of dissolved CO_2 as recharge water makes its way through the subsurface and reacts with bedrock (Drever 1997). Additional

research is needed to fully evaluate this interpretation, but if accurate, it is consistent with our findings and implies that mineral weathering shifts deeper into the subsurface in response to woody encroachment.

The transition zone where mineral concentrations shift from that of unweathered bedrock to weathered rock/regolith is sensitive to climate and land cover changes and plays a crucial role in secondary porosity development, thereby influencing hydrologic flow paths (Brantley et al. 2017). Thus, understanding catchment co-evolution necessitates comprehending the evolution and inter-relationship of hydrological flow paths and biogeochemical fluxes over time. This overarching inquiry is closely tied to an important question of the Anthropocene: How have human activities accelerated the evolution of subsurface environments (Singha et al. 2024)? For instance, if the deepening of roots from woody plants in formerly herbaceous systems prompts enhanced root and microbial respiration, organic-acid exudation or water fluxes at greater depths, the deepening of nested reaction fronts into the subsurface prompted by woody encroachment may alter the trajectory of catchment co-evolution.

5 | Conclusions

Our results showed that woody encroachment in a tallgrass prairie resulted in elevated coarse-root abundance and effective porosity well into the B horizon. These direct impacts of woody shrubs on soil structure created greater saturated hydraulic conductivity at the woody-encroached sites compared to grassy sites. Shifts in root abundance with land cover change will likely modify K_{sat} throughout the rooted profile over time—a dynamic process that is not well-defined in hydrologic models. Additionally, changes in soil structure and root size can impact infiltration and drainage of precipitation by altering flow pathways and subsurface hydrologic connectivity. Our analysis of ER during simulated rainfall events revealed distinctions in the lateral and vertical extent of water flow beneath shrubs and grasses. We also found faster flow rates and deeper penetration of water beneath shrubs compared to grasses. Our results underscore the impact of land cover change on shaping soil hydrological processes and the significance of woody encroachment on ecohydrological functioning of grassland ecosystems. Defining changes to soil water flow paths and soil water redistribution following woody encroachment will be important for predicting and modelling future changes in water cycling as well as the biogeochemical functioning of woody-encroached landscapes, including subsurface weathering and carbon and nutrient cycling.

Author Contributions

Karla M. Jarecke: conceptualisation, design, data collection, data analysis, writing. **Xi Zhang**: data collection, data analysis, editing. **Rachel M. Keen**: conceptualisation, data collection, editing. **Marc Dumont**: design, data collection, data analysis, editing. **Bonan Li**: design, data analysis, editing. **Kayalvizhi Sadayappan**: editing. **Victoria Moreno**: data collection, data analysis. **Hoori Ajami**: conceptualisation, editing. **Sharon A. Billings**: conceptualisation, editing. **Alejandro N. Flores**: conceptualisation. **Daniel R. Hirmas**: conceptualisation, editing. **Matthew F. Kirk**: editing. **Li Li**: conceptualisation, editing. **Jesse B. Nippert**: conceptualisation, data collection, editing. **Kamini Singha**: conceptualisation, design, data analysis, editing, supervision. **Pamela L Sullivan**: conceptualisation, design, data collection, data analysis, editing, supervision.

Acknowledgements

Data Availability Statement

Soil properties and soil moisture, soil temperature and electrical-resistivity time-series data are available on the Konza Prairie Biological Station database and the Environmental Data Initiative Data Portal (10.6073/pasta/da20d2d735876f97b84f212bc78ceb46).

References

Acharya, B. S., Y. Hao, T. E. Ochsner, and C. B. Zou. 2017. "Woody Plant Encroachment Alters Soil Hydrological Properties and Reduces Downward Flux of Water in Tallgrass Prairie." *Plant and Soil* 414, no. 1–2: 379–391. https://doi.org/10.1007/s11104-016-3138-0.

Angers, D. A., and J. Caron. 1998. "Plant-Induced Changes in Soil Structure: Processes and Feedbacks." *Biogeochemistry* 42: 55–72.

Anhold, C. 2023. "Impacts of Woody Encroachment on the Fate of Soil CO_2 in Grassland Watersheds [Thesis]." Kansas State University.

Araki, R., F. Branger, I. Wiekenkamp, and H. McMillan. 2022. "A Signature-Based Approach to Quantify Soil Moisture Dynamics Under Contrasting Land-Uses." *Hydrological Processes* 36, no. 4: e14553. https://doi.org/10.1002/hyp.14553.

Archer, S. R., E. M. Anderson, K. I. Predick, S. Schwinning, R. J. Steidl, and S. R. Woods. 2017. "Woody Plant Encroachment: Causes and Consequences." In *Rangland Systems: Processes, Management, and Challenges*, 25–84. Cham, Switzerland: Springer.

Banwart, S. A., N. P. Nikolaidis, Y.-G. Zhu, C. L. Peacock, and D. L. Sparks. 2019. "Soil Functions: Connecting Earth's Critical Zone." *Annual Review of Earth and Planetary Sciences* 47, no. 1: 333–359. https://doi.org/10.1146/annurev-earth-063016-020544.

Bargués Tobella, A., H. Reese, A. Almaw, et al. 2014. "The Effect of Trees on Preferential Flow and Soil Infiltrability in an Agroforestry Parkland in Semiarid Burkina Faso." *Water Resources Research* 50, no. 4: 3342–3354. https://doi.org/10.1002/2013WR015197.

Baver, L. D. 1939. "Soil Permeability in Relation to Non-Capillary Porosity." *Soil Science Society of America Journal* 3, no. C: 52–56. https://doi.org/10.2136/sssaj1939.036159950003000C0010x.

Berry, R. S., and A. Kulmatiski. 2017. "A Savanna Response to Precipitation Intensity." *PLoS ONE* 12, no. 4: e0175402. https://doi.org/10.1371/journal.pone.0175402.

Beven, K., and P. Germann. 2013. "Macropores and Water Flow in Soils Revisited." *Water Resources Research* 49, no. 6: 3071–3092. https://doi.org/10.1002/wrcr.20156.

Billings, S. A., D. Hirmas, P. L. Sullivan, et al. 2018. "Loss of Deep Roots Limits Biogenic Agents of Soil Development That Are Only Partially Restored by Decades of Forest Regeneration." *Elementa: Science of the Anthropocene* 6: 34. https://doi.org/10.1525/elementa.287.

Blanchy, G., S. Saneiyan, J. Boyd, P. McLachlan, and A. Binley. 2020. "ResIPy, an Intuitive Open Source Software for Complex Geoelectrical Inversion/Modeling." *Computers & Geosciences* 137: 104423. https://doi.org/10.1016/j.cageo.2020.104423.

Bogner, C., D. Gaul, A. Kolb, I. Schmiedinger, and B. Huwe. 2010. "Investigating Flow Mechanisms in a Forest Soil by Mixed-Effects Modelling." *European Journal of Soil Science* 61, no. 6: 1079–1090. https://doi.org/10.1111/j.1365-2389.2010.01300.x.

Brantley, S. L., M. I. Lebedeva, V. N. Balashov, K. Singha, P. L. Sullivan, and G. Stinchcomb. 2017. "Toward a Conceptual Model Relating Chemical Reaction Fronts to Water Flow Paths in Hills." *Geomorphology* 277: 100–117. https://doi.org/10.1016/j.geomorph.2016.09.027.

Burgess, S. S. O., M. A. Adams, N. C. Turner, D. A. White, and C. K. Ong. 2001. "Tree Roots: Conduits for Deep Recharge of Soil Water." *Oecologia* 126, no. 2: 158–165. https://doi.org/10.1007/s004420000501.

Case, M. F., and A. C. Staver. 2018. "Soil Texture Mediates Tree Responses to Rainfall Intensity in African Savannas." *New Phytologist* 219, no. 4: 1363–1372. https://doi.org/10.1111/nph.15254.

Craine, J. M., and J. B. Nippert. 2014. "Cessation of Burning Dries Soils Long Term in a Tallgrass Prairie." *Ecosystems* 17, no. 1: 54–65. https://doi.org/10.1007/s10021-013-9706-8.

Denef, K., J. Six, R. Merckx, and K. Paustian. 2002. "Short-Term Effect of Biological and Physical Forces on Aggregate Formation in Soils With Different Clay Mineralogy." *Plant and Soil* 246, no. 2: 185–200. https://doi.org/10.1023/A:1020668013524.

Deng, Y., X. Li, F. Shi, and X. Hu. 2021. "Woody Plant Encroachment Enhanced Global Vegetation Greening and Ecosystem Water-Use Efficiency." *Global Ecology and Biogeography* 30, no. 12: 2337–2353. https://doi.org/10.1111/geb.13386.

Devitt, D. A., and S. D. Smith. 2002. "Root Channel Macropores Enhance Downward Movement of Water in a Mojave Desert Ecosystem." *Journal of Arid Environments* 50, no. 1: 99–108. https://doi.org/10.1006/jare.2001.0853.

Dexter, A. R. 2004. "Soil Physical Quality Part I. Theory, Effects of Soil Texture, Density, and Organic Matter, and Effects on Root Growth." *Geoderma* 120: 201–214.

Dexter, A. R., and N. R. A. Bird. 2001. "Methods for Predicting the Optimum and the Range of Soil Water Contents for Tillage Based on the Water Retention Curve." *Soil and Tillage Research* 57, no. 4: 203–212. https://doi.org/10.1016/S0167-1987(00)00154-9.

Dodds, W. K., G. Wichman, J. P. Guinnip, J. R. Corman, and J. M. Blair. 2022. "Assessing Transport and Retention of Nitrate and Other Materials Through the Riparian Zone and Stream Channel With Simulated Precipitation." *Methods in Ecology and Evolution* 13, no. 3: 757–766. https://doi.org/10.1111/2041-210X.13791.

D'Odorico, P., G. S. Okin, and B. T. Bestelmeyer. 2012. "A Synthetic Review of Feedbacks and Drivers of Shrub Encroachment in Arid Grasslands." *Ecohydrology* 5, no. 5: 520–530. https://doi.org/10.1002/eco.259.

Drever, J. I. 1997. *The Geochemistry of Natural Waters: Surface and Groundwater Environments*, 3rd ed. Upper Saddle River, New Jersey, USA: Prentice Hall.

Eck, D. V., M. Qin, D. R. Hirmas, D. Giménez, and N. A. Brunsell. 2016. "Relating Quantitative Soil Structure Metrics to Saturated Hydraulic Conductivity." *Vadose Zone Journal* 15, no. 1: 1–11. https://doi.org/10.2136/vzj2015.05.0083.

Edwards, L. S. 1977. "A Modified Pseudosection for Resistivity and IP." *Geophysics* 42, no. 5: 1020–1036. https://doi.org/10.1190/1.1440762.

García Criado, M., I. H. Myers-Smith, A. D. Bjorkman, C. E. R. Lehmann, and N. Stevens. 2020. "Woody Plant Encroachment Intensifies Under Climate Change Across Tundra and Savanna Biomes." *Global Ecology and Biogeography* 29, no. 5: 925–943. https://doi.org/10.1111/geb.13072.

Garré, S., M. Javaux, J. Vanderborght, L. Pagès, and H. Vereecken. 2011. "Three-Dimensional Electrical Resistivity Tomography to Monitor Root Zone Water Dynamics." *Vadose Zone Journal* 10, no. 1: 412–424. https://doi.org/10.2136/vzj2010.0079.

Gee, G. W., and D. Or. 2002. "Particle-Size Analysis." In *Methods of Soil Analysis. Part 4. Physical Methods*, edited by J. H. Dane and C. G. Topp, 255–293. Madison, Wisconsin, USA: SSSA.

Ghestem, M., R. C. Sidle, and A. Stokes. 2011. "The Influence of Plant Root Systems on Subsurface Flow: Implications for Slope Stability." *Bioscience* 61, no. 11: 869–879. https://doi.org/10.1525/bio.2011.61.11.6.

Grossman, R., and T. Reinsch. 2002. "2.1 Bulk Density and Linear Extensibility." *Methods of Soil Analysis: Part 4 Physical Methods* 5: 201–228.

Guo, L., G. J. Mount, S. Hudson, H. Lin, and D. Levia. 2020. "Pairing Geophysical Techniques Improves Understanding of the Near-Surface Critical Zone: Visualization of Preferential Routing of Stemflow Along Coarse Roots." *Geoderma* 357: 113953. https://doi.org/10.1016/j.geoderma.2019.113953.

Gyssels, G., J. Poesen, E. Bochet, and Y. Li. 2005. "Impact of Plant Roots on the Resistance of Soils to Erosion by Water: A Review." *Progress in Physical Geography: Earth and Environment* 29, no. 2: 189–217. https://doi.org/10.1191/0309133305pp443ra.

Han, H., D. Giménez, and A. Lilly. 2008. "Textural Averages of Saturated Soil Hydraulic Conductivity Predicted From Water Retention Data." *Geoderma* 146, no. 1–2: 121–128. https://doi.org/10.1016/j.geoderma.2008.05.017.

Hardie, M., S. Lisson, R. Doyle, and W. Cotching. 2013. "Determining the Frequency, Depth and Velocity of Preferential Flow by High Frequency Soil Moisture Monitoring." *Journal of Contaminant Hydrology* 144, no. 1: 66–77. https://doi.org/10.1016/j.jconhyd.2012.10.008.

Hardie, M. A., W. E. Cotching, R. B. Doyle, G. Holz, S. Lisson, and K. Mattern. 2011. "Effect of Antecedent Soil Moisture on Preferential Flow in a Texture-Contrast Soil." *Journal of Hydrology* 398, no. 3–4: 191–201. https://doi.org/10.1016/j.jhydrol.2010.12.008.

Hatley, C. M., B. Armijo, K. Andrews, C. Anhold, J. B. Nippert, and M. F. Kirk. 2023. "Intermittent Streamflow Generation in a Merokarst Headwater Catchment." *Environmental Science: Advances* 2, no. 1: 115–131. https://doi.org/10.1039/D2VA00191H.

Hauser, E., P. L. Sullivan, A. N. Flores, D. Hirmas, and S. A. Billings. 2022. "Global-Scale Shifts in Rooting Depths Due to Anthropocene Land Cover Changes Pose Unexamined Consequences for Critical Zone Functioning. *Earth's*." *Futures* 10, no. 11: e2022EF002897. https://doi.org/10.1029/2022EF002897.

Hayley, K., L. R. Bentley, M. Gharibi, and M. Nightingale. 2007. "Low Temperature Dependence of Electrical Resistivity: Implications for Near Surface Geophysical Monitoring." *Geophysical Research Letters* 34, no. 18: L18402. https://doi.org/10.1029/2007GL031124.

Hirmas, D. R., H. Ajami, M. Sena, et al. In review. Predicting Macroporosity and Hydraulic Conductivity Dynamics: A Model for Integrating Laser-Scanned Profile Imagery With Soil Moisture Sensor Data.

Hirmas, D. R., and R. D. Mandel. 2017. *Soils of the Great Plains. Soils of the USA*, 131–163. Chichester, UK: Wiley.

Holdrege, M. C., K. H. Beard, and A. Kulmatiski. 2021. "Woody Plant Growth Increases With Precipitation Intensity in a Cold Semiarid System." *Ecology* 102, no. 1: e03212. https://doi.org/10.1002/ecy.3212.

Hu, H., J. Wen, Z. Peng, et al. 2019. "High-Frequency Monitoring of the Occurrence of Preferential Flow on Hillslopes and Its Relationship With

Rainfall Features, Soil Moisture and Landscape." *Hydrological Sciences Journal* 64, no. 11: 1385–1396. https://doi.org/10.1080/02626667.2019.1638513.

Huxman, T. E., B. P. Wilcox, D. D. Breshears, et al. 2005. "Ecohydrological Implications of Woody Plant Encroachment." *Ecology* 86, no. 2: 308–319. https://doi.org/10.1890/03-0583.

Johnson, M. S., and J. Lehmann. 2006. "Double-Funneling of Trees: Stemflow and Root-Induced Preferential Flow." *Écoscience* 13, no. 3: 324–333. https://doi.org/10.2980/i1195-6860-13-3-324.1.

Johnson, W. C., K. L. Willey, and G. L. Macpherson. 2007. "Carbon Isotope Variation in Modern Soils of the Tallgrass Prairie: Analogues for the Interpretation of Isotopic Records Derived From Paleosols." *Quaternary International* 162-163: 3–20. https://doi.org/10.1016/j.quaint.2006.10.036.

Jurena, P. N., and S. Archer. 2003. "Woody Plant Establishment and Spatial Heterogeneity in Grasslands." *Ecology* 84, no. 4: 907–919. https://doi.org/10.1890/0012-9658(2003)084[0907:WPEASH]2.0.CO;2.

Keen, R. M., J. B. Nippert, P. L. Sullivan, et al. 2022. "Impacts of Riparian and Non-Riparian Woody Encroachment on Tallgrass Prairie Ecohydrology." *Ecosystems* 26: 290–301. https://doi.org/10.1007/s10021-022-00756-7.

Keen, R. M., K. Sadayappan, K. M. Jarecke, et al. 2024. "Unexpected Hydrologic Response to Ecosystem State Change in Tallgrass Prairie." *Journal of Hydrology* 643: 131937. https://doi.org/10.1016/j.jhydrol.2024.131937.

Klute, A., and C. Dirksen. 1986. "Hydraulic Conductivity and Diffusivity: Laboratory Methods." In *Methods of Soil Analysis. Part 1. Physical and Mineralogical Methods*, 2nd ed., 687–734. Madison, Wisconsin, USA: Soil Science Society of America (SSSA) and American Society of Agronomy (ASA).

Kulmatiski, A., and K. H. Beard. 2013. "Woody Plant Encroachment Facilitated by Increased Precipitation Intensity." *Nature Climate Change* 3, no. 9: 833–837. https://doi.org/10.1038/nclimate1904.

LaBrecque, D. J., and X. Yang. 2001. "Difference Inversion of ERT Data: A Fast Inversion Method for 3-D in Situ Monitoring." *Journal of Environmental and Engineering Geophysics* 6, no. 2: 83–89. https://doi.org/10.4133/JEEG6.2.83.

Levia, D. F., and E. E. Frost. 2003. "A Review and Evaluation of Stemflow Literature in the Hydrologic and Biogeochemical Cycles of Forested and Agricultural Ecosystems." *Journal of Hydrology* 274, no. 1–4: 1–29. https://doi.org/10.1016/S0022-1694(02)00399-2.

Li, X.-Y., Z.-P. Yang, Y.-T. Li, and H. Lin. 2009. "Connecting Ecohydrology and Hydropedology in Desert Shrubs: Stemflow as a Source of Preferential Flow in Soils." *Hydrology and Earth System Sciences* 13, no. 7: 1133–1144.

Lin, H. S., K. J. McInnes, L. P. Wilding, and C. T. Hallmark. 1999. "Effects of Soil Morphology on Hydraulic Properties: I. Quantification of Soil Morphology." *Soil Science Society of America Journal* 63, no. 4: 948–954. https://doi.org/10.2136/sssaj1999.634948x.

Lu, J., Q. Zhang, A. D. Werner, Y. Li, S. Jiang, and Z. Tan. 2020. "Root-Induced Changes of Soil Hydraulic Properties—A Review." *Journal of Hydrology* 589: 125203. https://doi.org/10.1016/j.jhydrol.2020.125203.

Luo, L., H. Lin, and J. Schmidt. 2010. "Quantitative Relationships Between Soil Macropore Characteristics and Preferential Flow and Transport." *Soil Science Society of America Journal* 74, no. 6: 1929–1937. https://doi.org/10.2136/sssaj2010.0062.

Macpherson, G. L. 1996. "Hydrogeology of Thin Limestones: The Konza Prairie Long-Term Ecological Research Site, Northeastern Kansas." *Journal of Hydrology* 186: 191–228.

Macpherson, G. L. 2009. "CO_2 Distribution in Groundwater and the Impact of Groundwater Extraction on the Global C Cycle." *Chemical Geology* 264, no. 1–4: 328–336. https://doi.org/10.1016/j.chemgeo.2009.03.018.

Macpherson, G. L., and P. L. Sullivan. 2019. "Watershed-Scale Chemical Weathering in a Merokarst Terrain, Northeastern Kansas, USA." *Chemical Geology* 527: 118988. https://doi.org/10.1016/j.chemgeo.2018.12.001.

Macpherson, G. L., P. L. Sullivan, R. L. Stotler, and B. S. Norwood. 2019. "Increasing Groundwater CO_2 in a Mid-Continent Tallgrass Prairie: Controlling Factors." *E3S web of Conferences* 98: 06008. https://doi.org/10.1051/e3sconf/20199806008.

Nimmo, J. R. 2021. "The Processes of Preferential Flow in the Unsaturated Zone." *Soil Science Society of America Journal* 85, no. 1: 1–27. https://doi.org/10.1002/saj2.20143.

Nimmo, J. R., K. S. Perkins, K. M. Schmidt, D. M. Miller, J. D. Stock, and K. Singha. 2009. "Hydrologic Characterization of Desert Soils With Varying Degrees of Pedogenesis: 1. Field Experiments Evaluating Plant-Relevant Soil Water Behavior." *Vadose Zone Journal* 8, no. 2: 480–495. https://doi.org/10.2136/vzj2008.0052.

Nippert, J. B. 2024. "AWE01 Meteorological Data From the Konza Prairie Headquarters Weather Station [Dataset]." Environmental Data Initiative. https://doi.org/10.6073/pasta/910469efbf1f7e8d54c2b1ca864edec9.

Nippert, J. B., L. Telleria, P. Blackmore, J. H. Taylor, and R. C. O'Connor. 2021. "Is a Prescribed Fire Sufficient to Slow the Spread of Woody Plants in an Infrequently Burned Grassland? A Case Study in Tallgrass Prairie." *Rangeland Ecology & Management* 78: 79–89. https://doi.org/10.1016/j.rama.2021.05.007.

O'Keefe, K., D. M. Bell, K. A. McCulloh, and J. B. Nippert. 2020. "Bridging the Flux gap: Sap Flow Measurements Reveal Species-Specific Patterns of Water use in a Tallgrass Prairie." *Journal of Geophysical Research: Biogeosciences* 125, no. 2: e2019JG005446. https://doi.org/10.1029/2019JG005446.

Oldenburg, D. W., and Y. Li. 1999. "Estimating Depth of Investigation in DC Resistivity and IP Surveys." *Geophysics* 64, no. 2: 403–416. https://doi.org/10.1190/1.1444545.

R Core Team. 2023. "_R: A Language and Environment for Statistical Computing_. R Foundation for Statistical Computing [Computer software]." https://www.R-project.org/.

Ratajczak, Z., J. B. Nippert, and T. W. Ocheltree. 2014. "Abrupt Transition of Mesic Grassland to Shrubland: Evidence for Thresholds, Alternative Attractors, and Regime Shifts." *Ecology* 95, no. 9: 2633–2645. https://doi.org/10.1890/13-1369.1.

Reidmiller, D. R., C. W. Avery, D. R. Easterling, et al. 2017. *Impacts, Risks, and Adaptation in the United States: Fourth National Climate Assessment, Volume II*. Washington, D.C., USA: U.S. Global Change Research Program;National Oceanic and Atmospheric Administration;National Aeronuatics and Space Administration. https://doi.org/10.7930/NCA4.2018.

Sadayappan, K., R. Keen, K. M. Jarecke, et al. 2023. "Drier Streams Despite a Wetter Climate in Woody-Encroached Grasslands." *Journal of Hydrology* 627: 130388. https://doi.org/10.1016/j.jhydrol.2023.130388.

Schaap, M. G., F. J. Leij, and M. T. Van Genuchten. 2001. "Rosetta: A Computer Program for Estimating Soil Hydraulic Parameters With Hierarchical Pedotransfer Functions." *Journal of Hydrology* 251, no. 3–4: 163–176. https://doi.org/10.1016/S0022-1694(01)00466-8.

Schneider, C. A., W. S. Rasband, and K. W. Eliceiri. 2012. "NIH Image to ImageJ: 25 Years of Image Analysis." *Nature Methods* 9, no. 7: 671–675. https://doi.org/10.1038/nmeth.2089.

Scholl, P., D. Leitner, G. Kammerer, W. Loiskandl, H.-P. Kaul, and G. Bodner. 2014. "Root Induced Changes of Effective 1D Hydraulic Properties in a Soil Column." *Plant and Soil* 381, no. 1–2: 193–213. https://doi.org/10.1007/s11104-014-2121-x.

Schwärzel, K., S. Ebermann, and N. Schalling. 2012. "Evidence of Double-Funneling Effect of Beech Trees by Visualization of Flow

Pathways Using Dye Tracer." *Journal of Hydrology* 470–471: 184–192. https://doi.org/10.1016/j.jhydrol.2012.08.048.

Singha, K., P. L. Sullivan, S. A. Billings, et al. 2024. "Expanding the Spatial Reach and Human Impacts of Critical Zone Science." *Earth's Future* 12, no. 3: e2023EF003971. https://doi.org/10.1029/2023EF003971.

Soil Survey Staff. n.d. "Natural Resources Conservation Service, United States Department of Agriculture." Web Soil Survey. Accessed [3/21/2024]. Available Online at the Following Link: http://websoilsurvey.sc.egov.usda.gov/.

Sullivan, P. L., S. A. Billings, D. Hirmas, et al. 2022. "Embracing the Dynamic Nature of Soil Structure: A Paradigm Illuminating the Role of Life in Critical Zones of the Anthropocene." *Earth-Science Reviews* 225: 103873. https://doi.org/10.1016/j.earscirev.2021.103873.

Sullivan, P. L., M. W. Stops, G. L. Macpherson, L. Li, D. R. Hirmas, and W. K. Dodds. 2019. "How Landscape Heterogeneity Governs Stream Water Concentration-Discharge Behavior in Carbonate Terrains (Konza Prairie, USA)." *Chemical Geology* 527: 118989. https://doi.org/10.1016/j.chemgeo.2018.12.002.

Sullivan, P. L., C. Zhang, M. Behm, F. Zhang, and G. L. Macpherson. 2020. "Toward a new Conceptual Model for Groundwater Flow in Merokarst Systems: Insights From Multiple Geophysical Approaches." *Hydrological Processes* 34, no. 24: 4697–4711. https://doi.org/10.1002/hyp.13898.

Troch, P. A., T. Lahmers, A. Meira, et al. 2015. "Catchment Coevolution: A Useful Framework for Improving Predictions of Hydrological Change?" *Water Resources Research* 51, no. 7: 4903–4922. https://doi.org/10.1002/2015WR017032.

Tromp-van Meerveld, H. J., and J. J. McDonnell. 2006. "Threshold Relations in Subsurface Stormflow: 2. The Fill and Spill Hypothesis." *Water Resources Research* 42, no. 2: W02411. https://doi.org/10.1029/2004WR003800.

Twidwell, D., S. D. Fuhlendorf, C. A. Taylor, and W. E. Rogers. 2013. "Refining Thresholds in Coupled Fire-Vegetation Models to Improve Management of Encroaching Woody Plants in Grasslands." *Journal of Applied Ecology* 50, no. 3: 603–613. https://doi.org/10.1111/1365-2664.12063.

US Department of Agriculture. 2023. "Geospatial Data Getaway [Dataset]." https://datagateway.nrcs.usda.gov/.

Van Auken, O. W. 2009. "Causes and Consequences of Woody Plant Encroachment Into Western North American Grasslands." *Journal of Environmental Management* 90, no. 10: 2931–2942. https://doi.org/10.1016/j.jenvman.2009.04.023.

van Genuchten, M. 1980. "A Closed-Form Equation for Predicting the Hydraulic Conductivity of Unsaturated Soils." *Soil Science Society of America Journal* 44: 892–898.

Vero, S. E., G. L. Macpherson, P. L. Sullivan, et al. 2017. "Developing a Conceptual Framework of Landscape and Hydrology on Tallgrass Prairie: A Critical Zone Approach." *Vadose Zone Journal* 17, no. 1: 1–11. https://doi.org/10.2136/vzj2017.03.0069.

Watson, K. W., and R. J. Luxmoore. 1986. "Estimating Macroporosity in a Forest Watershed by Use of a Tension Infiltrometer." *Soil Science Society of America Journal* 50, no. 3: 578–582.

Wen, H., P. L. Sullivan, S. A. Billings, et al. 2022. "From Soils to Streams: Connecting Terrestrial Carbon Transformation, Chemical Weathering, and Solute Export Across Hydrological Regimes." *Water Resources Research* 58, no. 7: e2022WR032314. https://doi.org/10.1029/2022WR032314.

Wen, H., P. L. Sullivan, G. L. Macpherson, S. A. Billings, and L. Li. 2021. "Deepening Roots can Enhance Carbonate Weathering by Amplifying CO$_2$-Rich Recharge." *Biogeosciences* 18, no. 1: 55–75. https://doi.org/10.5194/bg-18-55-2021.

Wiekenkamp, I., J. A. Huisman, H. R. Bogena, H. S. Lin, and H. Vereecken. 2016. "Spatial and Temporal Occurrence of Preferential Flow in a Forested Headwater Catchment." *Journal of Hydrology* 534: 139–149. https://doi.org/10.1016/j.jhydrol.2015.12.050.

Wilcox, B. P., S. Basant, H. Olariu, and P. A. M. Leite. 2022. "Ecohydrological Connectivity: A Unifying Framework for Understanding how Woody Plant Encroachment Alters the Water Cycle in Drylands." *Frontiers in Environmental Science* 10: 934535. https://doi.org/10.3389/fenvs.2022.934535.

Wind, G. P. 1968. "Capillary Conductivity Data Estimated by a Simple Method." In *Water in the Unsaturated Zone. Proceedings of the Wageningen Symposium (Vol. 1, pp. 181–191)*, edited by P. E. Rijtema and H. Wassink. Wageningen, the Netherlands: IASAH.

Xiao, D., S. L. Brantley, and L. Li. 2021. "Vertical Connectivity Regulates Water Transit Time and Chemical Weathering at the Hillslope Scale." *Water Resources Research* 57, no. 8: e2020WR029207. https://doi.org/10.1029/2020WR029207.

Zhang, X., J. Zhu, O. Wendroth, C. Matocha, and D. Edwards. 2019. "Effect of Macroporosity on Pedotransfer Function Estimates at the Field Scale." *Vadose Zone Journal* 18, no. 1: 1–15. https://doi.org/10.2136/vzj2018.08.0151.

Zhang, Y., J. Niu, X. Yu, W. Zhu, and X. Du. 2015. "Effects of Fine Root Length Density and Root Biomass on Soil Preferential Flow in Forest Ecosystems." *Forestry Systems* 24, no. 1: 012. https://doi.org/10.5424/fs/2015241-06048.

Supporting Information

Additional supporting information can be found online in the Supporting Information section.